Aus der Klinik für Neurologie
der Medizinischen Fakultät Charité – Universitätsmedizin Berlin

DISSERTATION

MRT Biomarker für Perfusion und Infarktdemarkierung: Arterial Spin Labeling und DWI-Quantifizierung bei Patienten mit chronischen und akuten zerebrovaskulären Erkrankungen

zur Erlangung des akademischen Grades
Doctor medicinae (Dr. med.)

vorgelegt der Medizinischen Fakultät
Charité – Universitätsmedizin Berlin

von

Matthias Anthony Mutke

aus San Antonio, Vereinigte Staaten von Amerika

Datum der Promotion: 10.03.2017

Inhaltsverzeichnis

Abstrakt

Die evidenzbasierte Therapie von Patienten mit akutem Schlaganfall und chronischen zerebrovaskulären Erkrankungen basiert bisher vor allem auf allgemeinen Parametern wie der Zeit seit Symptombeginn oder dem Grad einer symptomatischen Stenose. Eine individuelle Diagnostik mittels MRT Bildgebung kann potentiell mehr Patienten eine wirksame Therapie ermöglichen. Die MRT Bildgebung muss jedoch schnell, sicher und zuverlässig anwendbar sein. Wir evaluierten daher neue diagnostische MRT Biomarker bei Patienten mit chronischen und akuten zerebrovaskulären Erkrankungen: Arterial Spin Labeling (ASL) ist eine kontrastmittelfreie und deshalb nebenwirkungsarme MRT Sequenz zur Messung einer zerebralen Hypoperfusion. In Arbeit 1 demonstrierten wir an 28 Patienten die Anwendung einer klinischen ASL Sequenz bei Patienten mit einer Stenose oder Okklusion der ACI oder ACM. Verzögerter Blutfluss zeigte sich als hyperintenses, so genanntes Arterial Transit Delay Artefact (ATDA). Zugleich ist das häufige ATDA aufgrund des hyperintensen Signals verantwortlich für eine schwache Korrelation bei der quantifizierten Messung der Hirnperfusion im Vergleich zur kontrastmittelbasierten Referenzmethode DSC-PWI. In Arbeit 2 testeten wir eine optimierte ASL Sequenz: Durch eine Korrektur für Blutflussverzögerungen verbesserte sich die Korrelation der Perfusionsmessung deutlich. In Arbeit 3 wurde ein weiterer etablierter MRT Biomarker getestet: Mittels DWI MRT in Kombination mit FLAIR MRT Sequenzen lässt sich der Zeitraum seit Infarktbeginn in Unkenntnis des Symptombeginnes abschätzen und erlaubt eine Zuordnung zum Thrombolysezeitfenster. Die visuelle FLAIR Diagnostik ist jedoch im Gegensatz zur DWI aufgrund niedriger Rater-Übereinstimmung potentiell unzuverlässig. Wir testeten daher eine Quantifizierung des DWI-Signals: Ein DWI Grenzwert von 162% der Signalintensität im Vergleich zur gesunden Hemisphäre erlaubt die Detektion von Patienten, die bereits eine FLAIR Demarkation zeigen. Diese Ergebnisse ermöglichen eine Einschätzung des Infarktbeginnes durch die alleinige Auswertung des DWI Signals. Die Kombination von DWI und ASL könnte eine schnelle, sichere und zuverlässige Evaluation des potentiell therapierelevanten Gewebes erlauben.

Abstract

In acute stroke and chronic cerebrovascular diseases, evidence-based therapeutic decisions depend mostly on parameters such as time from symptom onset or grading of a symptomatic stenosis. Individual diagnostics with MR Imaging may include more patients amenable to treatment. To that end, MRI must be fast, safe and reliable. Considering these criteria, we evaluated new diagnostic biomarkers in patients with acute and chronic cerebrovascular diseases: Arterial Spin Labeling (ASL) is a non-invasive MRI sequence for measuring cerebral hypoperfusion with minimal side-effects. In publication 1, we showed its applicability in 28 patients with stenosis or occlusion of the ICA and MCA. Delayed blood flow is visible as an Arterial Transit Delay Artefact (ATDA). The ATDA could be established as a qualitative diagnostic sign for a cerebral hypoperfusion. Because of its hyperintense nature, there was a low correlation of the quantified ASL-CBF measurement compared with a standard DSC-PWI sequence. In publication 2, we tested an optimized ASL sequence: By correcting for delayed blood flow, the correlation of the brain perfusion measurement improved significantly. Another established MRI Biomarker is DWI, showing irreversibly infarcted tissue immediately after symptom onset. In combination with the delayed appearance of FLAIR lesions, symptom onset can be estimated and matched with the thrombolysis time window. Visual inspection of FLAIR lesions is potentially unreliable as opposed to DWI evaluation. In publication 3 we therefore quantified the DWI signal: A threshold of 162% of the DWI signal intensity as opposed to the healthy hemisphere reliably detects a corresponding FLAIR lesion. This allows for the assessment of the symptom onset by DWI alone. A combination of DWI and ASL securely and quickly detects potentially treatment relevant tissue.

Einführung

Patienten mit akutem Schlaganfall oder chronischen zerebrovaskulären Erkrankungen wie Stenosen oder Okklusionen der A. carotis interna und der A. cerebri media werden bisher meist aufgrund von statischen, streng formulierten Parametern therapiert. Dadurch wird jedoch oft eine wirksame Therapie vorenthalten: Bei chronischen Gefäßstenosen zeigt beispielsweise ein verminderter CBF ein erhöhtes Schlaganfallrisiko[1] an, oft basiert eine Therapie jedoch nur auf dem morphologischen Stenosegrad[2]. Auch beim akuten Schlaganfall ist eine intravenöse Thrombolyse nur innerhalb von 4.5 Stunden zugelassen. Dieses Zeitfenster wurde ausschließlich epidemiologisch etabliert und erfordert immer die Beobachtung des Symptombeginns oder des letzten symptomfreies Zeitpunktes[3]. Potentielles Risikogewebe, dass durch rasche Therapie vor einer ansonsten endgültigen Nekrose bewahrt werden kann, ist jedoch weit außerhalb des 4.5 Stunden Zeitfensters nachgewiesen[4] und kann durch multimodale MRT Bildgebung individuell dargestellt werden: Der Perfusions/Diffusionsmismatch (gemessen mit DWI/PWI MRT) identifiziert regional verminderten zerebralem Blutfluss (CBF) in Kombination mit der Messung des irreversibel geschädigten Infarktkernes[5].

Therapieentscheidungen bei Patienten mit akuten und chronischen zerebrovaskulären Erkrankungen lassen sich damit potentiell anhand des individuellen Gewebezustandes und abseits eines generalisierenden Zeitfensters oder rein morphologischer Parameter treffen.

MRT Bildgebung muss jedoch für eine Translation in die klinische Routine einfach und zuverlässig sowie für den Patienten sicher einsetzbar sein. Dieses Kriterium ist bei der Messung des CBF nicht erfüllt. Die DSC-PWI Sequenz erfordert die Injektion eines exogenen Kontrastmittels auf Gadolinium-Basis: Diese Kontrastmittel können bei Patienten mit Niereninsuffizienz eine nephrogene systemische Sklerose hervorrufen[6] und ist daher für diese Patienten kontraindiziert. Alle Patienten sind zudem der Gefahr einer allergischen Reaktion ausgesetzt. Zudem verursacht Kontrastmittel zusätzliche Kosten. Mit Arterial Spin Labeling existiert eine alternative Form der CBF Messung, die kein exogenes Kontrastmittel benötigt[7].

Beim Arterial Spin Labeling werden im Blut enthaltene Protonen selektiv auf Halsebene invertiert und markiert (eng: labeled). Dadurch entsteht dort ein markierter

Blutbolus, der ins Hirngewebe einfließt. Seine Passagezeit zwischen Halsebene und Hirnkapillare ist die Arterial Transit Zeit (ATT, arterial transit time). Die Zeit zwischen Markierung und Bildakquisition innerhalb des Gehirns findet nach einer festgelegten Inversionszeit (TI, time of inversion) statt. Die ATT repräsentiert damit einen physiologischen bzw. bei Verlängerung einen pathophysiologischen Parameter, die TI ist eine rein technische, bei der Bildakquisition einstellbare Größe. Für eine fehlerfreie Messung und Quantifizierung des CBF ist ein vollständiger Einfluss des markierten Blutbolus in das zerebrale Kapillarbett und eine vollständige Diffusion bis zum Erreichen eines Flussgleichgewichts notwendig, d.h. die TI sollte im Idealfall länger als die ATT sein. Nach Bildakquisition mit Labeling des Blutes wird eine Kontrollbild erstellt, aus der Differenz dieser Bilder lässt sich der zerebrale Blutfluss errechnen.

Eine einfache und zuverlässige Anwendung von ASL war jedoch bisher erschwert: Aufgrund der Komplexität der Methodik kommen in Studien bisher fast ausschließlich Forschungssequenzen zum Einsatz. Für eine Translation in die klinische Routine ist die Validierung von kommerziell erhältlichen und standardisierten Sequenzen notwendig[8]. Wir testeten daher zur Darstellung des CBF bei Patienten mit Stenosen oder Okklusionen der hirnversorgenden Gefäße zunächst eine kommerziell verfügbare ASL Sequenz, die jederzeit in der klinischen Routine einsetzbar ist. In einer Folgestudie wurde eine hierauf basierende, optimierte ASL Sequenz getestet, auch diese kann mittlerweile in der Routinebildgebung verwendet werden.

Ein weiterer Biomarker für das irreversibel infarzierte Hirngewebe bei Patienten mit akutem Schlaganfall ist die kombinierte Evaluation der DWI und der FLAIR MRT Sequenzen. Bei einem DWI/FLAIR Mismatch (sichtbare DWI Hyperintensität ohne korrespondierende FLAIR Hyperintensität) kann der Zeitpunkt des Infarktes einem Zeitfenster kleiner 4.5 Stunden zugeordnet werden und könnte eine intravenöse Thrombolyse bei unklarem Symptombeginn ermöglichen[9]. Die visuelle Identifikation von FLAIR Läsionen ist fehleranfällig und weist im Gegensatz zur Detektion einer DWI Läsion eine schlechtere Interraterreliabilität auf[10]. Ein ausschließlich auf der DWI basierender Biomarker könnte zuverlässiger und potentiell automatisiert gemessen werden. Wir testeten daher, ob die quantitative Analyse des DWI-Signals die FLAIR-Information bereits beinhaltet und ob das DWI Signal eine Abhängigkeit von der Zeit seit Symptombeginn aufweist.

Das Ziel der gesamten Promotion ist eine methodologische Basis für klinische Translationsstudien, die eine Kombination von ASL und DWI nutzen. So könnten potentiell einfache, schnelle und sichere Therapieentscheidungen bei mehr Patienten möglich werden.

Eigene Arbeiten

Originalarbeit 1

Klinische Evaluation einer Arterial-Spin-Labeling Produktsequenz bei Stenosen und Okklusionen der Hirngefäße.

Clinical Evaluation of an Arterial-Spin-Labeling Product Sequence in Steno-Occlusive Disease of the Brain

Matthias A. Mutke , Vince I. Madai , Federico C. von Samson-Himmelstjerna, Olivier Zaro Weber, Gajanan S. Revankar, Steve Z. Martin, Katharina L. Stengl, Miriam Bauer, Stefan Hetzer, Matthias Günther, Jan Sobesky.

PLoS One. 2014 Feb 6;9(2):e87143. doi: 10.1371/journal.pone.0087143. eCollection 2014.

Wir testeten die Messung des CBF durch eine ASL-Produktsequenz für Siemens-MRTs (PICORE Q2TIPS)[11] im Vergleich zum klinischen Standard DSC-PWI innerhalb einer prospektiven Bildgebungsstudie (PEGASUS). Die vorliegende Arbeit ist die erste Studie, die den klinischen Nutzen einer Produktsequenz in diesem Patientenkollektiv evaluiert.

Wesentliche Einschlusskriterien der Studie waren eine unilaterale Stenose der ACI oder der ACM größer als 70%. 28 Patienten wurden in einem 3 Tesla MRT (Magnetom Trio, Siemens Healthcare) gemessen.

ASL-CBF maps wurden ohne weitere Nachbearbeitung direkt aus der MRT-Konsole übernommen, um die klinische Anwendung zu simulieren. Aus den DSC-PWI Daten wurden DSC-CBF sowie DSC-TTP (time to peak) maps erstellt. DSC-TTP visualisiert den Zeitraum bis zur maximalen Konzentration des Kontrastmittels und ist damit ein Surrogat für die Verzögerungen des Blutflusses.

ASL-CBF, DSC-CBF und DSC-TTP wurden visuell von drei Untersuchern hinsichtlich Bildqualität sowie Hyper-, Hypo- und normaler Intensität bewertet. Auf ASL-CBF maps wurde das Arterial Transit Delay Artefact (ATDA) beachtet: Das ATDA ist ein Hinweis auf verzögerte Ankunft des markierten Blutes[12]. Es visualisiert sich als stark hyperintense Areale mit punktförmigem oder geschlängeltem Aspekt, deren

Umgebung einen Signalverlust bzw. starke Hypointensität aufweist (s. Grafik 5 in der Originalarbeit).

Nach Koregistrierung auf anatomische MR-Sequenzen wurde sowohl eine Region of Interest (ROI) und eine Volume of Interest (VOI) Auswertung stratifiziert nach Gefäßterritorium (ACA, ACM, ACP) vorgenommen. Jeweils wurde ein relativer CBF (relCBF) in % für ASL und DSC-PWI berechnet (Verhältnis zur gesunden Hemisphäre für CBF, Differenz zur gesunden Hemisphäre für TTP).

Zusätzlich wurden anhand der visuellen Analyse ROIs mit und ohne korrespondierendes Auftreten des ATDA auf ASL-maps identifiziert.

In der visuellen Analyse zeigten sich 11 von 28 ASL maps aufgrund von Bewegungsartefakten als nicht interpretierbar. Auf den restlichen 17 von 28 maps fand sich bei 12 Patienten ein ATDA, welches bei 9 von 12 mit einer Hypoperfusion des DSC-CBF und bei 10 von 12 mit einer Verzögerung der DSC-TTP einherging. Die Korrelation zwischen DSC-CBF und ASL-CBF war in der ROI-Analyse nur schwach signifikant (Spearman's Rho=0.24, $p<0.05$), in der VOI Analyse der verschiedenen Gefäßterritorien fand sich kein signifikanter Zusammenhang. Im Bland-Altmann Plot zeigte sich eine Schwankung der ASL-CBF und DSC-CBF Werte zwischen -113% und +144%.

Originalarbeit 2

3D GRASE pulsed arterial spin labeling bei multiplen Einflusszeiten in Patienten mit langer arterieller Transitzeit: Vergleich mit Dynamic Susceptibility Weighted Contrast Enhanced 3 Tesla MRI.

3D GRASE pulsed arterial spin labeling at multiple inflow times in patients with long arterial transit times: Comparison with dynamic susceptibility-weighted contrast-enhanced MRI at 3 Tesla.

Steve Z. Martin, Vince I. Madai, Federico C. von Samson-Himmelstjerna, Matthias A. Mutke, Miriam Bauer, Cornelius X. Herzig, Stefan Hetzer, Matthias Günther and Jan Sobesky.

J Cereb Blood Flow Metab. 2015 Mar;35(3):392-401. doi:10.1038/jcbfm.2014.200. Epub 2014 Nov 19.

Die vorliegende Arbeit evaluiert eine ASL Sequenz (3D GRASE) mit Messung anhand mehrerer Inversionszeiten (in Zusammenarbeit mit Prof. Matthias Günther am Fraunhofer Institut für Bildgestützte Medien MEVIS)[13]. Diese Technik ermöglicht eine Korrektur für Blutflussverzögerungen.

43 Patienten mit Stenosen/Okklusionen der hirnversorgenden Gefäße wurden im Rahmen der PEGASUS-Studie in einem 3 Tesla Siemens MRT mittels ASL und DSC-PWI gemessen. Die pASL Akquisition erfolgte bei multiplen Inversionszeiten (von 0.3 bis 3.1 Sekunden mit jeweils 0.2 Sekunden Inkrement). Die zu unterschiedlichen Inversionszeiten gewonnenen ASL-Daten wurden an eine Modellfunktion angepasst (General Kinetic Model)[14] und daraus eine ASL-CBF map sowie eine ASL-BAT (bolus arrival time) map pro Patient erstellt. BAT maps visualisieren die Ankunft des mit ASL markierten Blutes: Die Voxelintensität repräsentiert den Zeitpunkt der erstmaligen Detektion eines ASL-Signals. Die Auswertung erfolgte analog zu Originalarbeit 1, ASL-CBF und ASL-BAT sowie DSC-CBF und DSC-TTP wurden durch drei Rater nach Gefäßterritorium (ACA, ACM, ACP) qualitativ analysiert. Nach Koregistrierung wurden eine ROI und eine VOI-basierte Auswertung ergänzt.

Alle Bilder konnten interpretiert und ausgewertet werden, ASL maps hatten eine deutlich verbesserte Bildqualität. Für ASL maps errechnete sich anhand der visuellen

Analyse eine gute Sensitivität von 82% (ACM-Stromgebiet) bzw. 75% (ACA-Stromgebiet) für die Detektion einer Hypoperfusion auf DSC-CBF maps. Im ACA Stromgebiet zeigte sich jedoch auf ASL-CBF maps bei 90% der Patienten eine rechtsseitige Hypointensität ohne korrelierendes Perfusionsdefizit. Ursache ist eine Verzerrung des Signals der EPI single shot Sequenz aufgrund von Inhomogenitäten des statischen Magnetfeldes. Wir identifizierten erstmalig diese Fehlerquelle und demonstrierten die Korrektur des Artefakts durch Bildakquisition in zwei entgegengesetzte Phasenkodierrichtungen. Dies führte in der vorliegenden Arbeit zu visuell deutlich verbesserten Ergebnissen.

Ein ATDA fand sich bei nur 12% der gemessenen Patienten. Die Korrelation zwischen ASL-CBF und DSC CBF für das ACM-Stromgebiet (Spearman's Rho=0.52 für ROI und rho=0.48 für VOI Auswertung) war signifikant und im Vergleich zu Arbeit 1 deutlich verbessert, bei schwach signifikanter Korrelation für das ACA und ACP Stromgebiet.

Originalarbeit 3

DWI Intensitätswerte prognostizieren FLAIR Läsionen beim akuten ischämischen Schlaganfall.

DWI Intensity Values Predict FLAIR Lesions in Acute Ischemic Stroke.

Vince I. Madai, Ivana Galinovic, Ulrike Grittner, Olivier Zaro-Weber, Alice Schneider, Steve Z. Martin, Federico C. v. Samson-Himmelstjerna, Katharina L. Stengl, Matthias A. Mutke, Walter Moeller-Hartmann, Martin Ebinger, Jochen B. Fiebach, Jan Sobesky.

PLoS One. 2014 Mar 21;9(3):e92295. doi: 10.1371/journal.pone.0092295.eCollection 2014.

Eine DWI Läsion ohne korrespondierende FLAIR Läsion im akuten Schlaganfall identifiziert Patienten mit einem Schlaganfallbeginn unter 4.5 Stunden[9] und erlaubt so eine Einschätzung des Gewebezustand („tissue clock"). Die Studie untersucht, ob anhand der Quantifizierung des DWI Signals eine Aussage über eine zusätzliche FLAIR Läsion getroffen werden kann.

In einer retrospektiven Bildgebungsstudie an zwei Zentren wurden insgesamt 97 Patienten (mit 1.5 und 3 Tesla MRT) untersucht. DWI und FLAIR maps wurden koregistriert. In einer visuellen Analyse mit drei Untersuchern wurde die gesamte FLAIR Läsion als ROI festgelegt und auf die DWI Läsion kopiert. Innerhalb der DWI Läsion wurden ebenfalls ROIs platziert, diese wurden als jeweils FLAIR positiv und FLAIR- negativ stratifiziert. DWI ROIs wurden anhand der gesunden Hemisphäre normalisiert (in %). Mittels ROC Analyse wurde ein Grenzwert für relative DWI Werte gesucht, ab dem eine begleitende FLAIR Läsion auftritt.

Der Grenzwert von 162% des relativen DWI-Signals konnte ein Schlaganfallbeginn größer als 4.5 Stunden mit guter AUC identifizierten (mean AUC bei 3 Untersuchern: 1.5T: 0.84, 3.0T: 0.87, mean AUC bei 3 Untersuchern: 1.5T: 0.84, 3.0T: 0.87). Der quantifizierte DWI Wert zeigte sich zudem abhängig vom Infarktbeginn (Korrelation DWI Signal/Zeit, Rho=0.54 für 1.5 Tesla und Rho=0.73 für 3 Tesla).

Diskussion

Die vorliegende Promotionsarbeit untersucht *1.* die **kontrastmittelfreie Messung der Hirnperfusion** (Arbeiten 1 und 2) mittels **Arterial Spin Labeling** bei Patienten mit chronischen Stenosen und Okklusionen der hirnzuführenden Gefäße und *2.* eine **Quantifizierung des DWI-Signals** zur Einschätzung des Gewebezustandes bei Patienten mit akutem ischämischen Schlaganfall und unklarem Symptombeginn (Arbeit 3).

Arterial Spin Labeling nutzt das eigene Blut des Patienten zur nichtinvasiven Darstellung des CBF[7], für eine kurze technische Beschreibung s. Einführung. Die einfache Anwendung von ASL wird durch die Diversität der Sequenzen und die Komplexität der einzelnen Akquisitionsparameter erschwert. Bisherige Studien bei Patienten mit chronischen Stenosen oder Okklusionen der ACI oder ACM nutzten ausschließlich Forschungssequenzen, die für den klinischen Einsatz nicht zugelassen sind. Die Translation in die klinische Anwendung wird ausdrücklich gefordert[8]. Wir testeten daher in Arbeit 1 explizit eine kommerziell verfügbare, für den klinischen Einsatz zertifizierte ASL-Sequenz ohne weitere Modifikation oder Nachbearbeitung (PICORE ASL). PICORE ASL misst den zerebralen Blutfluss anhand einer singulären TI, d.h. die Bildakquise findet zu einem fixen Zeitpunkt statt. Bei Patienten mit Stenosen und Okklusionen ist jedoch die tatsächliche Ankunftszeit des Blutes, die Arterial Transit Zeit, verzögert und zudem interindividuell sehr unterschiedlich.

In der qualitativen Analyse zeigte sich ein Arterial Transit Delay Artefact (ATDA oder auch Arterial Transit Artifact, ATA). Es entsteht durch eine verlängerte Arterial Transit Time. Bei Bildakquisition hat das markierte Blut die Kapillare noch nicht erreicht und zeigt sich als stark hyperintenses Signal, das auf engem Raum in präkapillären Gefäßen punkt- oder strichförmig konzentriert ist, s. Grafik 5 in Originalarbeit 1. Areale mit ATDA auf ASL maps zeigten eine signifikante Verzögerung der Kontrastmittelankunftszeit auch auf DSC-TTP maps. Das ATDA kann daher als diagnostischer Biomarker zur Identifikation von Blutflussverzögerungen bei Patienten mit Stenosen oder Okklusionen der ACI oder der ACM genutzt werden. Darüber hinaus hat das ATDA einen positiv prädiktiven Wert von 75% für eine ipsilaterale CBF Minderung gemessen mit DSC-CBF.

Während das ATDA einen guten visuellen Biomarker für Blutflussverzögerung darstellt, beeinflusst es die quantitative Korrelation des ASL-CBF mit dem DSC-CBF. Durch die Hyperintensität des ATDA korreliert der gemessene Wert nicht mit einer entsprechenden Hypoperfusion auf den DSC-CBF maps.

PICORE-ASL zeigte sich anfällig für Bewegungsartefakte. Da aufgrund der 2D EPI Akquisition die Sequenz für ein ausreichendes Signal-Rausch Verhältnis mehrfach durchgeführt werden muss, führt eine Bewegung des Kopfes zu entsprechenden Qualitätseinbußen.

In Arbeit 2 wurde eine verbesserte ASL-Sequenz (3D GRASE ASL) am gleichen Patientenkollektiv wie in Arbeit 1 getestet. Zwei wesentliche Neuerungen bestehen:

- 3D GRASE ASL misst bei mehreren TIs. Das Signal kann so über mehrere Zeitpunkte verfolgt werden. Die höchste gemessene TI liegt bei 3.1 Sekunden und damit 1.3 Sekunden länger als bei PICORE ASL.
- Die Bildakquisition erfolgt mittels 3D EPI single shot, das Signal-Rausch Verhältnis ist deutlich größer.

Die Ergebnisse zeigen, dass 3D GRASE ASL weniger anfällig für Bewegungs- sowie Arterial Transit Delay Artefakte ist. Die Korrelation zwischen DSC-CBF und ASL-CBF konnte im Gegensatz zum in Arbeit 1 verwendeten PICORE-ASL deutlich verbessert werden. Es fand sich jedoch eine erhöhte Distorsion des ASL-Bildes aufgrund der rechts-links EPI-Akquisition. Wir konnten erstmalig eine einfache Korrektur entwickeln, die allerdings mit einer aufwendigeren Nachbearbeitung verbunden ist.

Die Synopsis beider Arbeiten demonstriert, dass für die Translation in die klinische Routine optimale ASL Parameter beachtet werden müssen. Insbesondere die Arterial Transit Time spielt eine zentrale Rolle. Dies spiegelt sich in international konsentierten Empfehlungen wieder[15]. Zudem konnte die sichere, schnelle und nichtinvasive Anwendung von ASL demonstriert werden. Mit einer Akquisitionszeit von ca. 2 Minuten ist die ASL Sequenz schnell in ein Schlaganfall-Bildgebungsprotokoll integrierbar.

Ein Biomarker zur Darstellung des Infarktalters ist die Kombination aus DWI und FLAIR MRT bei Patienten mit akutem ischämischem Schlaganfall und unklarem Symptombeginn.

Diese Methode basiert auf einem visuellen Eindruck, bei der Detektion der FLAIR Läsionen ist die Interraterreliabilität jedoch eine mögliche Fehlerquelle[10]. Quantifizierte Methoden sind unabhängig von subjektiven Einflüssen und potentiell automatisierbar. In Arbeit 3 konnte gezeigt werden, dass ein Grenzwert von 162% der relativen DWI Signalintensität (DWI rSI) mit guter Sensitivität und Spezifität eine FLAIR Läsion anzeigt und so die Zuordnung zum 4.5 Stunden Zeitfenster ermöglicht. Zusätzlich fand sich eine Korrelation von erhöhtem DWI Signal und Symptombeginn. Diese Ergebnisse lassen vermuten, dass die Intensität des DWI Signals ab Symptombeginn ansteigt und ein Surrogat für die Vitalität des Gewebes ist.

Eine Kombination von ASL und einem quantifiziertem DWI-Signal stellt individuell das Risikogewebe bei Patienten mit chronischen und akuten zerebrovaskulären Erkrankungen dar. Die vorliegende Promotionsarbeit konnte demonstrieren, dass diese Biomarker einfach, schnell und sicher messbar sind. Dies ermöglicht weiterführende Studien zur Therapieentscheidungen, um mehr Patienten unter Nutzung spezifischer pathophysiologischer Informationen behandeln zu können.

Literaturverzeichnis

1. Yamauchi H, Higashi T, Kagawa S, Nishii R, Kudo T, Sugimoto K, Okazawa H, Fukuyama H.
Is misery perfusion still a predictor of stroke in symptomatic major cerebral artery disease?
Brain. 2012;135:2515–2526.

2. Meschia JF, Bushnell C, Boden-Albala B, Braun LT, Bravata DM, Chaturvedi S, Creager MA, Eckel RH, Elkind MSV, Fornage M, Goldstein LB, Greenberg SM, Horvath SE, Iadecola C, Jauch EC, Moore WS, Wilson JA.
Guidelines for the Primary Prevention of Stroke A Statement for Healthcare Professionals From the American Heart Association/American Stroke Association.
Stroke. 2014;45:3754–3832.

3. Lees KR, Bluhmki E, von Kummer R, Brott TG, Toni D, Grotta JC, Albers GW, Kaste M, Marler JR, Hamilton SA, Tilley BC, Davis SM, Donnan GA, Hacke W, Allen K, Mau J, Meier D, del Zoppo G, De Silva DA, Butcher KS, Parsons MW, Barber PA, Levi C, Bladin C, Byrnes G.
Time to treatment with intravenous alteplase and outcome in stroke: an updated pooled analysis of ECASS, ATLANTIS, NINDS, and EPITHET trials.
Lancet. 2010;375:1695–1703.

4. González RG, Hakimelahi R, Schaefer PW, Roccatagliata L, Sorensen AG, Singhal AB.
Stability of large diffusion/perfusion mismatch in anterior circulation strokes for 4 or more hours.
BMC Neurol. 2010;10:13.

5. Sobesky J.
Refining the mismatch concept in acute stroke: lessons learned from PET and MRI.
J. Cereb. Blood Flow Metab. Off. J. Int. Soc. Cereb. Blood Flow Metab. 2012;32:1416–1425.

6. Kaewlai R, Abujudeh H.
Nephrogenic systemic fibrosis.
AJR Am. J. Roentgenol. 2012;199:W17–23.

7. Williams DS, Detre JA, Leigh JS, Koretsky AP.
Magnetic resonance imaging of perfusion using spin inversion of arterial water.
Proc. Natl. Acad. Sci. U. S. A. 1992;89:212–216.

8. Zaharchuk G.
Arterial Spin Labeling for Acute Stroke: Practical Considerations.
Transl. Stroke Res. 2012;3:228–235.

9. Thomalla G, Cheng B, Ebinger M, Hao Q, Tourdias T, Wu O, Kim JS, Breuer L, Singer OC, Warach S, Christensen S, Treszl A, Forkert ND, Galinovic I, Rosenkranz M, Engelhorn T, Köhrmann M, Endres M, Kang D-W, Dousset V, Sorensen AG, Liebeskind DS, Fiebach JB, Fiehler J, Gerloff C, STIR and VISTA

Imaging Investigators.
DWI-FLAIR mismatch for the identification of patients with acute ischaemic stroke within 4·5 h of symptom onset (PRE-FLAIR): a multicentre observational study.
Lancet Neurol. 2011;10:978–986.

10. Galinovic I, Puig J, Neeb L, Guibernau J, Kemmling A, Siemonsen S, Pedraza S, Cheng B, Thomalla G, Fiehler J, Fiebach JB.
Visual and region of interest-based inter-rater agreement in the assessment of the diffusion-weighted imaging- fluid-attenuated inversion recovery mismatch.
Stroke J. Cereb. Circ. 2014;45:1170–1172.

11. Luh W, Wong EC, Bandettini PA, Hyde JS.
QUIPSS II with thin-slice TI1 periodic saturation: A method for improving accuracy of quantitative perfusion imaging using pulsed arterial spin labeling.
Magn. Reson. Med. 1999;41:1246–1254.

12. Telischak NA, Detre JA, Zaharchuk G.
Arterial spin labeling MRI: Clinical applications in the brain.
J. Magn. Reson. Imaging. 2015;41:1165–1180.

13. Günther M, Oshio K, Feinberg DA.
Single-shot 3D imaging techniques improve arterial spin labeling perfusion measurements.
Magn. Reson. Med. 2005;54:491–498.

14. Buxton RB, Frank LR, Wong EC, Siewert B, Warach S, Edelman RR.
A general kinetic model for quantitative perfusion imaging with arterial spin labeling.
Magn. Reson. Med. 1998;40:383–396.

15. Alsop DC, Detre JA, Golay X, Günther M, Hendrikse J, Hernandez-Garcia L, Lu H, MacIntosh BJ, Parkes LM, Smits M, van Osch MJP, Wang DJJ, Wong EC, Zaharchuk G.
Recommended implementation of arterial spin-labeled perfusion MRI for clinical applications: A consensus of the ISMRM perfusion study group and the European consortium for ASL in dementia.
Magn. Reson. Med. 2013;n/a–n/a.

Abkürzungen

3D GRASE	3 dimensional gradient and spin echo
ACA	Arteria cerebri anterior
ACI	Arteria carotis interna
ACM	Arteria cerebri media
ACP	Arteria cerebri posterior
ASL	Arterial Spin Labeling
ATDA	Arterial Transit Delay Artifact
ATT	Arterial Transit Time
AUC	Area Under the Curve
BAT	Bolus Arrival Time
CBF	Cerebral Blood Flow
DSC-PWI	Dynamic Susceptibility Perfusion Weighted Imaging
TTP	Time To Peak
TI	Time of Inversion
DWI	Diffusion Weighted Imaging
ECST	European Carotid Surgery Trial
EPI	Echo Planar Imaging
FLAIR	Fluid Attenuated Inversion Recovery
MRT	Magnetresonanztomographie oder Magnetresonanztomograph
NIHSS	National Institute of Health Stroke Scale
pASL	Pulsed Arterial Spin Labeling
PEGASUS	Perfusion imaging by arterial spin labeling for clinical use in stroke
PICORE	Proximal Inversion with Control for Off-Resonance Effects
Q2TIPS	Quantitative Imaging of Perfusion using a Single Subtraction Second Version with thin-slice TI1 Periodic Saturation
relCBF	Relative Cerebral Blood Flow
ROC	Receiver Operating Characteristic
ROI	Region of Interest
sSVD	Standard Single Value Decomposition
VOI	Volume of Interest

Eidesstattliche Versicherung

„Ich, Matthias Anthony Mutke, versichere an Eides statt durch meine eigenhändige Unterschrift, dass ich die vorgelegte Dissertation mit dem Thema: **„Arterial Spin Labeling und DWI-Quantifizierung: MRT Biomarker bei Patienten mit chronischen und akuten zerebrovaskulären Erkrankungen“** selbstständig und ohne nicht offengelegte Hilfe Dritter verfasst und keine anderen als die angegebenen Quellen und Hilfsmittel genutzt habe.

Alle Stellen, die wörtlich oder dem Sinne nach auf Publikationen oder Vorträgen anderer Autoren beruhen, sind als solche in korrekter Zitierung (siehe „Uniform Requirements for Manuscripts (URM)“ des ICMJE -*www.**icmje**.org*) kenntlich gemacht. Die Abschnitte zu Methodik (insbesondere praktische Arbeiten, Laborbestimmungen, statistische Aufarbeitung) und Resultaten (insbesondere Abbildungen, Graphiken und Tabellen) entsprechen den URM (s.o) und werden von mir verantwortet.

Meine Anteile an den ausgewählten Publikationen entsprechen denen, die in der untenstehenden gemeinsamen Erklärung mit dem Betreuer angegeben sind. Sämtliche Publikationen, die aus dieser Dissertation hervorgegangen sind und bei denen ich Autor bin, entsprechen den URM (s.o) und werden von mir verantwortet.

Die Bedeutung dieser eidesstattlichen Versicherung und die strafrechtlichen Folgen einer unwahren eidesstattlichen Versicherung (§156,161 des Strafgesetzbuches) sind mir bekannt und bewusst.“

_____

Datum Unterschrift

Anteilserklärung an den erfolgten Publikationen

Matthias Anthony Mutke hatte folgenden Anteil an den folgenden Publikationen:

Publikation 1:

Clinical Evaluation of an Arterial-Spin-Labeling Product Sequence in Steno-Occlusive Disease of the Brain
Matthias A. Mutke , Vince I. Madai , Federico C. von Samson-Himmelstjerna, Olivier Zaro Weber, Gajanan S. Revankar, Steve Z. Martin, Katharina L. Stengl, Miriam Bauer, Stefan Hetzer, Matthias Günther, Jan Sobesky.

PLOS One, 2014
Feb 6;9(2):e87143. doi: 10.1371/journal.pone.0087143. eCollection 2014.

Beitrag im Einzelnen: Mitarbeit bei der Konzipierung der Studie und Erstellung der relevanten Anträge, Rekrutierung und Datenerhebung, Konzipierung und Durchführung der Auswertung sowie Erstellung des Manuskripts.

Publikation 2:

3D GRASE pulsed arterial spin labeling at multiple inflow times in patients with long arterial transit times: comparison with dynamic susceptibility-weighted contrast-enhanced MRI at 3 Tesla
Steve Z. Martin, Vince I. Madai, Federico C. von Samson-Himmelstjerna, Matthias A. Mutke, Miriam Bauer, Cornelius X. Herzig, Stefan Hetzer, Matthias Günther and Jan Sobesky.

Journal of Cerebral Blood Flow & Metabolism, 2015
Mar;35(3):392-401. doi: 10.1038/jcbfm.2014.200. Epub 2014 Nov 19.

Beitrag im Einzelnen: Mitarbeit an der Konzipierung der Studie, Erstellung der relevanten Anträge, Konzipierung der Auswertung sowie Mitarbeit bei der Dateninterpretation und am Manuskript.

Publikation 3:

DWI Intensity Values Predict FLAIR Lesions in Acute Ischemic Stroke

Vince I. Madai, Ivana Galinovic, Ulrike Grittner, Olivier Zaro-Weber, Alice Schneider, Steve Z. Martin, Federico C. v. Samson-Himmelstjerna, Katharina L. Stengl, Matthias A. Mutke, Walter Moeller-Hartmann, Martin Ebinger, Jochen B. Fiebach, Jan Sobesky.

PLOS One, 2014

Mar 21;9(3):e92295. doi: 10.1371/journal.pone.0092295. eCollection 2014.

Beitrag im Einzelnen: Mitarbeit bei der Datenerhebung und der Erstellung des Manuskriptes.

Unterschrift, Datum und Stempel des betreuenden Hochschullehrers/der betreuenden Hochschullehrerin

_____

Unterschrift des Doktoranden/der Doktorandin

_____

Eigene Arbeiten

OPEN ACCESS Freely available online

PLOS ONE

Clinical Evaluation of an Arterial-Spin-Labeling Product Sequence in Steno-Occlusive Disease of the Brain

Matthias A. Mutke[1,5☯], Vince I. Madai[1,5☯], Federico C. von Samson-Himmelstjerna[1,2,5], Olivier Zaro Weber[1,4,5], Gajanan S. Revankar[1], Steve Z. Martin[1,5], Katharina L. Stengl[1,5], Miriam Bauer[1,5], Stefan Hetzer[3], Matthias Günther[2], Jan Sobesky[1,5]*

1 Center for Stroke Research, Charité Universitätsmedizin, Berlin, Germany, **2** Fraunhofer/MEVIS, Bremen, Germany, **3** Berlin Center for Advanced Neuroimaging, Berlin, Germany, **4** Max-Planck-Institute for Neurological Research, Cologne, Germany, **5** Department of Neurology, Charité Universitätsmedizin, Berlin, Germany

Abstract

Introduction: In brain perfusion imaging, arterial spin labeling (ASL) is a noninvasive alternative to dynamic susceptibility contrast-magnetic resonance imaging (DSC-MRI). For clinical imaging, only product sequences can be used. We therefore analyzed the performance of a product sequence (PICORE-PASL) included in an MRI software-package compared with DSC-MRI in patients with steno-occlusion of the MCA or ICA >70%.

Methods: Images were acquired on a 3T MRI system and qualitatively analyzed by 3 raters. For a quantitative analysis, cortical ROIs were placed in co-registered ASL and DSC images. Pooled data for ASL-cerebral blood flow (CBF) and DSC-CBF were analyzed by Spearman's correlation and the Bland-Altman (BA)-plot.

Results: In 28 patients, 11 ASL studies were uninterpretable due to patient motion. Of the remaining patients, 71% showed signs of delayed tracer arrival. A weak correlation for DSC-relCBF vs ASL-relCBF ($r = 0.24$) and a large spread of values in the BA-plot owing to unreliable CBF-measurement was found.

Conclusion: The PICORE ASL product sequence is sensitive for estimation of delayed tracer arrival, but cannot be recommended to measure CBF in steno-occlusive disease. ASL-sequences that are less sensitive to patient motion and correcting for delayed blood flow should be available in the clinical setting.

Citation: Mutke MA, Madai VI, von Samson-Himmelstjerna FC, Zaro Weber O, Revankar GS, et al. (2014) Clinical Evaluation of an Arterial-Spin-Labeling Product Sequence in Steno-Occlusive Disease of the Brain. PLoS ONE 9(2): e87143. doi:10.1371/journal.pone.0087143

Editor: Jeroen Hendrikse, University Medical Center (UMC) Utrecht, Netherlands

Received August 27, 2013; **Accepted** December 18, 2013; **Published** February 6, 2014

Funding: The research leading to these results has received funding from the German Federal Ministry of Education and Research via the grant "Center for Stroke Research Berlin" (01 EO 0801; http://www.bmbf.de). The funders had no role in study design, data collection and analysis, decision to publish, or preparation of the manuscript.

Competing Interests: JS reports the following board memberships, consultancies and/or payments for lectures including service on speaker's bureaus: Boehringer-Ingelheim, Bayer, Pfizer and Maquet. This does not alter the authors' adherence to all the PLOS ONE policies on sharing data and materials.

* E-mail: jan.sobesky@charite.de

☯ These authors contributed equally to this work.

Introduction

Cerebral blood flow (CBF) is an important measure of brain perfusion in patients with steno-occlusive disease [1]. Using magnetic resonance imaging (MRI), dynamic susceptibility-weighted contrast-enhanced (DSC) imaging is the clinical standard of CBF measurement. It is fast and offers a reliable estimate of CBF [2]. However, the main drawback of DSC imaging is the need of a gadolinium-based contrast agent. Administration of gadolinium is invasive, may cause anaphylaxis and patients with renal insufficiency must be excluded owing to possible nephrogenic systemic sclerosis [3]. Additionally, repeated measurements are difficult to perform owing to slow clearance of gadolinium based contrast agents [4]. Arterial spin labeling (ASL) measures CBF without the need of an exogenous contrast agent [5]. Here, blood is magnetically labeled by the MR scanner and the labeled blood water protons serve as an endogenous contrast agent to calculate CBF. ASL therefore permits multiple noninvasive CBF measurement. Various ASL techniques have been successfully validated to measure CBF in neuropathologies, e.g. in brain tumors [6], epilepsy [7] and stenosis of cerebral arteries and acute stroke [8]. Most of these sequences, however, were research sequences and are not available for clinical imaging. For clinical diagnosis, in contrast, available product sequences have to be used and their validation is urgently needed [9,10]. We therefore studied the performance of a clinically available commercial ASL-sequence to measure CBF in comparison with DSC-MRI in patients with steno-occlusive disease of the brain.

Materials and Methods

Ethics Statement

All patients gave informed written consent prior to the study. The study was conducted according to the principles expressed in the Declaration of Helsinki and was approved by the authorized

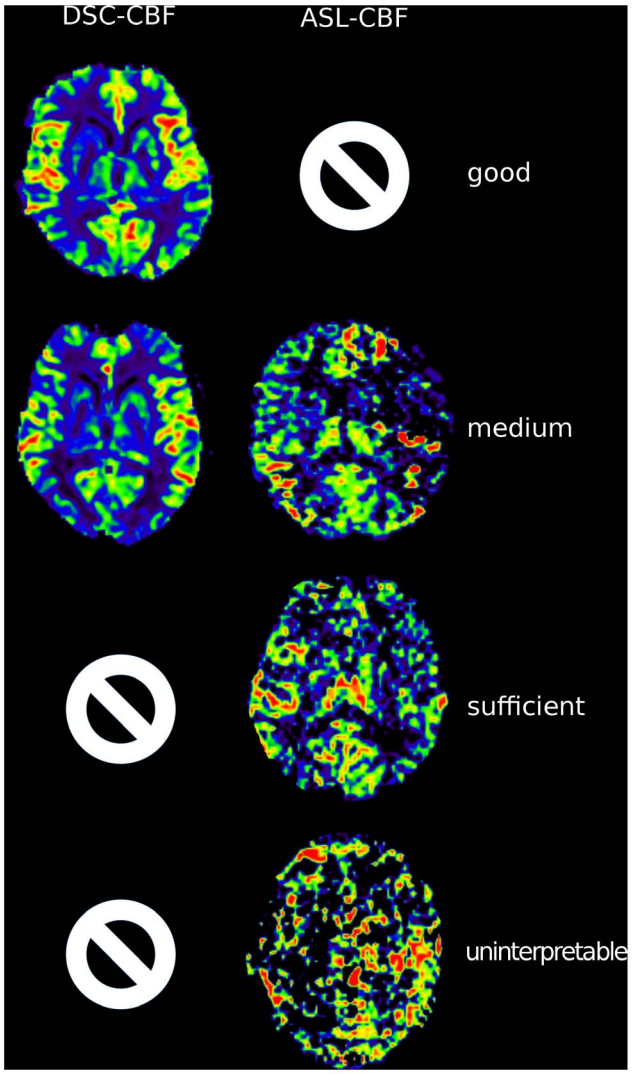

Figure 1. Rating of quality. The figure demonstrates the different image qualities. Rows show examples for good, medium, sufficient and uninterpretable quality. The first column demonstrates DSC-CBF images. All DSC-CBF maps were of either "good" or "medium" quality. The second column shows ASL-CBF images. No ASL-CBF map was rated "good".
doi:10.1371/journal.pone.0087143.g001

institutional review board (IRB) of the Charité - Universitätsmedizin Berlin.

Study Design

We performed an observational prospective imaging study (Perfusion imaging by arterial spin labeling for clinical use in stroke - PEGASUS, WHO international Clinical trials registry No. DRKS00003198). Patients with steno-occlusive disease were recruited at the Department of Neurology of the Charité - Universitätsmedizin Berlin or presenting at our out-patient services between September 2011 and November 2012. Inclusion criteria were: a) unilateral stenosis >70% of one internal carotid artery (ICA) or middle cerebral artery (MCA) according to the ECST (European Carotid Surgery Trial) criteria, b) age 18–80 and c) clinically and hemodynamically stable status. Grading of stenosis was confirmed prior to MRI by Duplex-Sonography and/or CT-angiography.

Exclusion criteria were a) contralateral stenosis >50% of the CCA (common carotid artery), ICA or MCA b) magnetic implants, c) claustrophobia, d) aphasia or reduced level of consciousness, e) severe allergic reactions in the previous medical history, f) allergic reactions against Gadolinium-based contrast agents in the past, g) renal insufficiency (defined by a GFR $\leq$30 ml/min/1,73 m^2), h) pregnancy and i) unstable clinical status. For each patient National Institute of Health Stroke Scale (NIHSS), modified Rankin Scale (mRS) and relevant clinical data was assessed before imaging.

Magnetic Resonance Imaging Hardware

MR-imaging was performed on a 3 T whole-body system (Magnetom Trio, Siemens Healthcare, Erlangen, Germany) using a 12-channel receive RF coil (Siemens Healthcare, Erlangen, Germany) tailored for head imaging.

Magnetic Resonance Imaging Sequences

We used a commercially available pulsed arterial spin labeling (PASL) PICORE Q2TIPS product sequence [11,12]: 50 pairs of label/control ASL images were acquired in axial direction at a single inversion time of 1800 ms (EPI-readout, TR = 2600 ms, TE = 13 ms, TI1 = 700 ms, label thickness = 100 mm, PICORE Q2T perfusion mode, voxel size: $3\times3\times5$ mm^3, no crusher gradients, enabled prospective motion correction [3D-PACE]).

The DSC-MRI protocol consisted of 80 series of whole-brain images using a single-shot FID-EPI sequence (TR = 1390 ms, TE = 29 ms, voxel size: $1.8\times1.8\times5$ mm^3) after injection of 5 ml Gadovist® (Gadobutrol, 1 M, Bayer Schering Pharma AG, Berlin) followed by 25 ml saline flush by a power injector (Spectris, Medrad Inc., Warrendale PA, USA) at a rate of 5 ml/s. Acquisition time for ASL was 4 min:18 s, for DSC-MRI 1 min:54 s. DSC-MRI was performed immediately after ASL.

Data Postprocessing

ASL images were acquired directly from the console and were used without further post-processing. DSC-MRI images were postprocessed offline with PMA (Perfusion Mismatch Analyzer, ASIST Japan, Iwate, Japan). Two maps were generated from the raw data: 1) DSC-time-to-peak (TTP)-maps -indicating regional delayed blood flow- and 2) DSC-CBF-maps – indicating regional blood flow - with automatic placement of the arterial input function using sSVD (standard singular value decomposition) deconvolution.

Qualitative Analysis

Maps of ASL-CBF, DSC-CBF and DSC-TTP were visually assessed by three readers blinded to clinical data (JS, 10 years experience in stroke perfusion imaging; VM, 3 years; MM, 2 years; all 3 readers have special expertise in ASL imaging).

A majority rating was reached if at least two raters applied the same rating. In cases where all three raters disagreed, all three obtained a consensus.

The rating was performed following a predefined standardized algorithm:

Imaging quality was rated as "good", "medium", "sufficient" or "uninterpretable" (Figure 1). Raters were asked to rate hyperintensities, hypointensities or normal intensity for each hemisphere on maps of ASL-CBF, DSC-CBF and DSC-TTP. On ASL-CBF images, raters were asked to note the appearance of artifacts owing to increased blood transit times, the "arterial transit delay artifact" (ATDA): It is defined by two signs: First, the occurrence of hyperintense lines or dots. Second, larger areas of severe

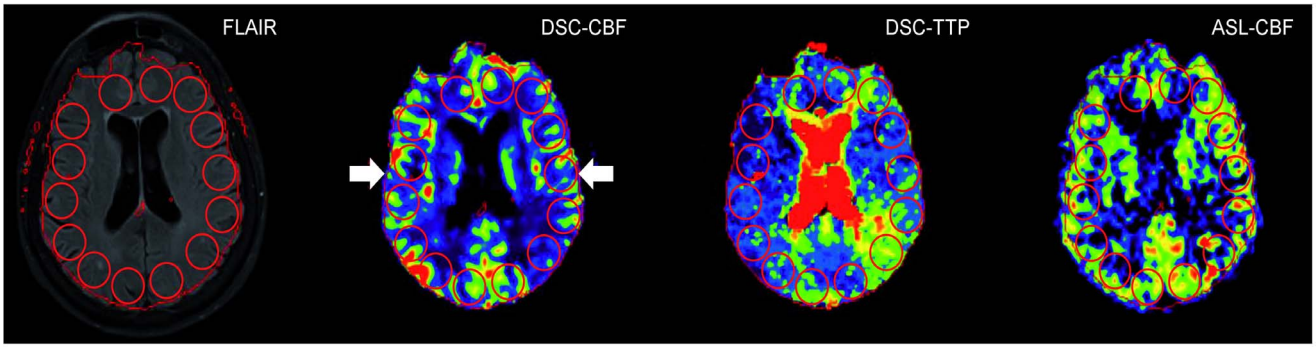

Figure 2. Quantitative analysis of DSC-CBF, DSC-TTP and ASL-relCBF. 20 mm circular regions of interest (ROIs) were placed on the FLAIR image and copied onto coregistered DSC-CBF, DSC-TTP and ASL images. For relative values, the ratio of each ipsilateral ROI to the arithmetic mean of all contralateral ROIs was calculated. In case of DSC-TTP the values were subtracted to obtain relative TTP-delay. DSC-perfusion maps were automatically masked by the used software. Therefore, the contour of DSC maps was used to define the cortical rim (contour, arrows).
doi:10.1371/journal.pone.0087143.g002

Table 1. Clinical data of all patients.

Patient number	sex	Age (y)	mRS (p)	NIHSS (p)	Barthel (p)	Stroke	TIA	GoS (%)	GoS (%)	GoS(%)	GoS(%)
								ICA re.	ICA li.	MCA re.	MCA li.
1	f	66	0	0	100			100			
2	m	63	0	0	100			70–80			
3	f	70	0	0	100		x		80		
4	f	79	2	3	100		x		70–80		
5	m	45	0	0	100	x			100		
6	f	45	1	1	100	x					100
7	f	56	0	0	100	x			100		
8	m	42	1	1	100		x			100	
9	f	50	0	0	100			100			
10	m	59	1	2	100	x		90			
11	f	57	0	0	100	x			100		
12	f	45	0	0	100		x	70			
13	m	63	2	4	100	x		80			
14	f	49	0	0	100	x		90			
15	f	36	2	2	100	x			100		
16	m	76	0	0	100	x		70			
17	m	31	0	0	100	x			100		
18	m	47	2	4	75	x		100			
19	f	63	0	0	100	x				70	
20	f	37	0	0	100				100		
21	f	73	0	0	100			70	30		
22	m	48	0	0	100				100		
23	m	46	0	0	100	x			100		
24	f	73	0	0	100		x		70–80		
25	m	65	0	0	100				100		
26	f	74	0	0	100			80			
27	m	58	0	0	100		x		>80		
28	m	68	0	0	100	x		70–80			

y: years; p: points; mRS: Modified Rankin Scale, NIHSS: National Institute of Health Stroke Scale; GoS: Grade of Stenosis; ICA: Internal Carotid Artery; MCA: Middle Cerebral Artery.
doi:10.1371/journal.pone.0087143.t001

Table 2. Visual rating of DSC-CBF/ASL.

		DSC-CBF		
		hypoperfusion	**normal**	
ASL	ATDA	9	3	(12)
	normal	2	3	(5)
		(11)	(6)	

Results of the visual qualitative analysis. As hypoperfusion in ASL occurred exclusively as part of ATDA and not isolated, for ASL only the categories ATDA and normal are presented.
Rows show imaging findings for ASL-CBF, columns show imaging findings for DSC-CBF. Patients rated uninterpretable were excluded.
Of 11 patients with hypoperfusion in DSC-CBF, 9 patients showed ATDAs in ASL (specificity: 82%; false negative rate: 18%). 6 patients had normal DSC-CBF findings, 3 of them showed ATDAs in ASL (false positive: 50%).
DSC-CBF: Dynamic Susceptibility Contrast - Cerebral Blood Flow; ASL: Arterial Spin Labeling; ATDA: Arterial Transit Delay Artifact.
doi:10.1371/journal.pone.0087143.t002

Table 3. Visual rating of TTP/ASL.

		TTP		
		delay	**normal**	
ASL	ATDA	10	2	(12)
	normal	4	1	(5)
		(14)	(3)	

Results of the visual qualitative analysis. As hypoperfusion in ASL occurred exclusively as part of ATDA and not isolated, for ASL only the categories ATDA and normal are presented.
Rows show imaging findings for ASL-CBF, columns show imaging findings for DSC-TTP. Patients rated uninterpretable were excluded. Of 14 patients with a TTP delay, 10 showed Arterial Transit Delay Artifacts in ASL (specificity: 71%; false negative rate: 29%). Out of 3 patients with normal findings in TTP, 1 showed ATDAs in ASL (false positive rate: 67%).
DSC-TTP: Dynamic Susceptibility Contrast - Time to Peak; ASL: Arterial Spin Labeling; ATDA: Arterial Transit Delay Artifact.
doi:10.1371/journal.pone.0087143.t003

hypoperfusion adjacent to the hyperintense areas [13]. (Both signs are are addressed in detail in the discussion).

Quantitative Analysis

For the quantitative analysis, ASL-images rated as "uninterpretable" were excluded. Coregistration and region of interest (ROI) placement was performed with VINCI 3.93 (Max-Planck Institute for Neurological Research, Cologne, Germany) [14].

Maps of ASL-CBF, DSC-CBF and DSC-TTP were coregistered with FLAIR as the reference image. Cortical ROIs (diameter: 20 mm) were placed on 7 consecutive axial slices located at the height of the lateral ventricles. Slices above the lateral ventricles and slices including the cerebellum were not included. ROIs were placed on FLAIR images and copied on all perfusion maps (Figure 2). ROIs were labeled according to the side of steno-occlusion (ipsi- or contralateral). Relative CBF values (relCBF) were calculated using the mean value of each ROI: (ipsilateral ROI value/mean of all contralateral ROIs on the same slice) [%]. The relative time to peak (relTTP) for ipsilateral ROIs was obtained by subtraction from the mean TTP of all contralateral ROIs. Negative voxel values were not included in the analysis.

In a following ROI-analysis, TTP-ROIs were divided in two groups: First, TTP-ROIs showing an ATDA in the corresponding ASL-ROI and second TTP-ROIs without ATDA in the corresponding ASL-ROI. For comparison, the relative TTP delay was calculated as described above.

In a further volumetric analysis, we segmented grey matter on MPRAGE (T1) maps using Mevislab (MeVis Medical Solutions AG, Bremen, Germany). The grey matter map was divided into three flow territories: ACA (anterior cerebral artery), MCA (middle cerebral artery), PCA (posterior cerebral artery) based on a brain perfusion atlas [15]. The grey matter maps were applied to co-registered ASL-CBF and DSC-CBF maps. The average value for a specific flow territory volume was normalized to the mean perfusion of the whole contralateral grey matter perfusion.

Statistical Analysis

Study data are given in median and interquartile range owing to skewed distribution of some variables if not indicated otherwise. In the ROI-analysis, values of ASL-relCBF were plotted against relTTP and DSC-relCBF and correlated using Spearman's rho. The Bland-Altman (BA) plot was used to compare values of ASL-relCBF vs. DSC-relCBF. Logarithmic BA plots were used, when measurement errors seemed to be proportional to the mean.

For the comparison of the relative TTP-delay of TTP-ROIs with ATDA vs. without ATDA on corresponding ROIs in ASL we used the Man-Whitney U test, since the distribution was skewed.

In the analysis of the grey matter perfusion, values of ASL-CBF and DSC-CBF were compared using Spearman's rho.

All statistical methods described were applied to pooled data from all patients. Statistical tests were performed with SigmaPlot 11 (Systat, San José, California, U.S.A.).

Results

28 patients met the inclusion criteria, all of them completed the imaging protocol.

Median age of all patients was 58 years, 20 patients had previous stroke or TIA. Detailed clinical data are shown in Table 1.

In the visual qualitative analysis, 11/28 ASL images were rated uninterpretable owing to severe patient motion artifacts, no ASL series was rated of good quality. In DSC-MRI in contrast, 13/28 image series were rated of good quality and only 1/28 DSC-TTP maps was rated as uninterpretable. In detail (good/medium/sufficient/uninterpretable): ASL (0/4/13/11); DSC-CBF (13/15/0/0), DSC-TTP (13/12/2/1). For the following analysis, patients with ASL measurements rated as "uninterpretable" were excluded resulting in 17 patients. 14/17 patients showed delay in DSC-TTP ipsilateral to the stenosis. In 10 of these 14 patients, ASL also showed delay by an arterial transit delay artifact (ATDA) (sensitivity: 71%). In DSC-CBF, 11/17 patients showed ipsilateral hypoperfusion. Corresponding ASL images identified ATDA in 9 of these patients (sensitivity: 81%). In ASL, hypoperfusion always occurred as part of ATDA, no isolated hypoperfusion without ATDA was found in ASL. Detailed results of the qualitative assessment are found in Table 2 and Table 3.

In the quantitative analysis, pooled data showed a weak correlation for DSC-relCBF vs ASL-relCBF ($r = 0.24$ [$p<0.05$]) and a weak negative correlation for DSC-relTTP vs ASL-relCBF ($r = -32$ [$p<0.05$]). Scatter plots are shown in Figure 3. The Bland Altman Plot showed a mean difference between DSC-relCBF and ASL-relCBF measurements of 13% relative difference with a high spread of values ranging from −113% to +144% relative difference. Negative differences were seen in low average

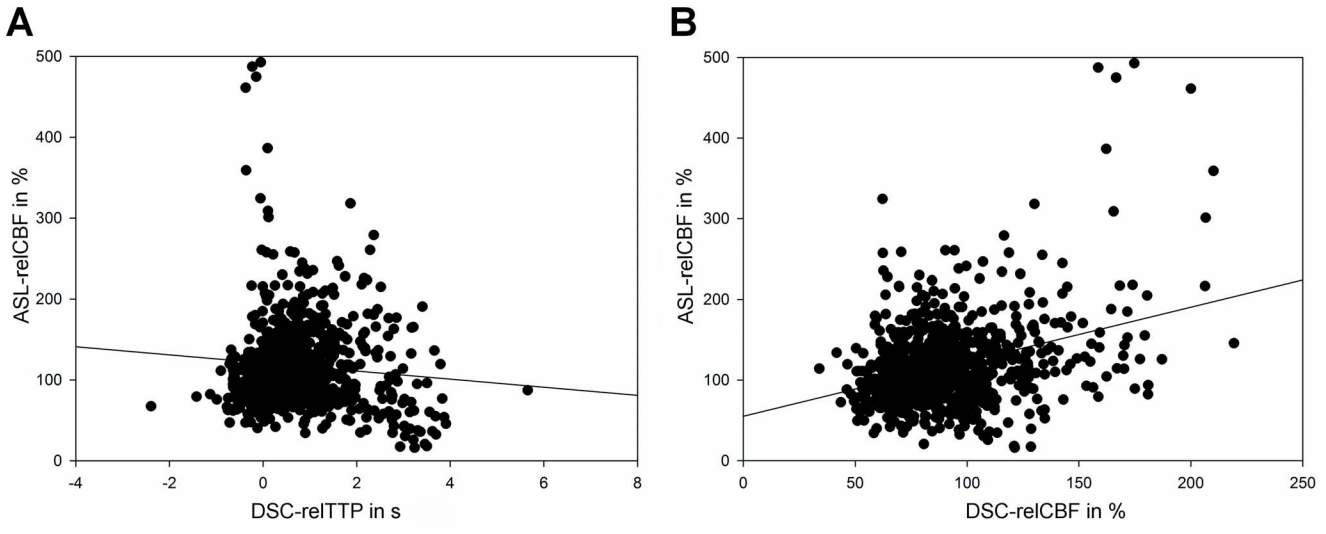

Figure 3. Scatter plots comparing DSC-relCBF and ASL-relCBF (A) and relTTP and ASL-relCBF (B). Pooled data of 17 patients. The diversity of the results is demonstrated in the two scatter plots. Spearman's rho for the pooled data was r = 0,24 ($p<0,05$) for DSC-relCBF vs ASL-relCBF and r = −0,32 ($p<0,05$) for relTTP vs ASL-relCBF.
doi:10.1371/journal.pone.0087143.g003

relCBF and high differences in high average relCBF, suggesting a proportional error. This was, however, not confirmed in a logarithmic transformation of the plot (data not shown). The Bland Altman Plot is shown in Figure 4.

TTP-ROIs with a corresponding ATDA on ASL had a significantly ($p<0.001$) longer median delay (1.9 sec) than those without a corresponding ATDA (0.6 sec).

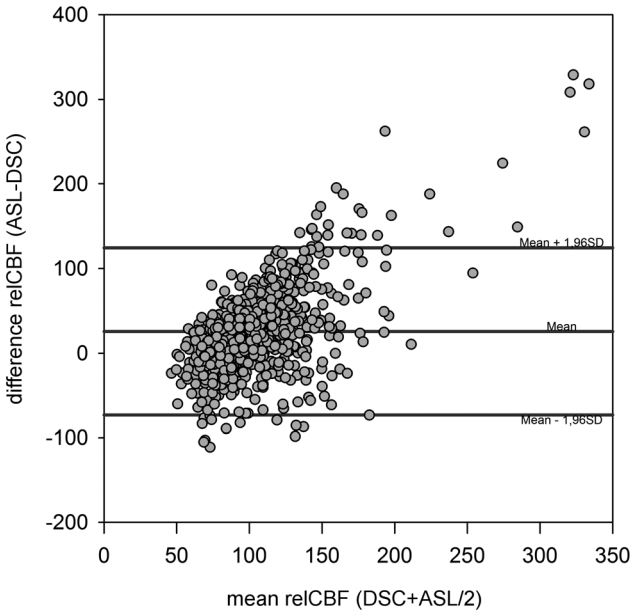

Figure 4. Bland-Altman-Plots comparing DSC-CBF and ASL-CBF. In the Bland Altman Plot, there is a large positive difference around 144% for high mean relCBF values between the two modalities. For low mean relCBF values, on the other hand, a large negative difference around −113% is seen. This pattern is suggestive of a proportional error. However, this was not confirmed by a logarithmic Bland-Altman Plot (not shown).
doi:10.1371/journal.pone.0087143.g004

In the volumetric grey matter analysis, for ASL-CBF and DSC-CBF no significant correlation was found for all three arterial flow territories (ACA: r = 0.01 [p = 0.97], MCA: r = −0.09 [p = 0.72], PCA: r = −0.05 [p = 0.85]).

Discussion

We report on the performance of an arterial spin labeling product sequence to measure CBF in patients with steno-occlusive disease in comparison with the clinical standard DSC-MRI. The tested ASL sequence is the only commercial, approved product sequence currently available for this system [10]. Sensitivity to patient motion made 39% of obtained ASL-images uninterpretable. In the visual analysis, ASL identified blood flow delay as defined by DSC-MRI with fair sensitivity, but led to unreliable measurement of CBF.

There is emerging consensus that ASL is a reliable alternative to exogenous contrast agent based perfusion measurements. Its use in routine clinical imaging has been encouraged [16]. However, most of the ASL techniques used for scientific neuroimaging are research sequences. This is important to note, as these sequences are usually not available in the clinical setting. Clinicians, who implement ASL in routine clinical imaging, currently are obliged to use commercially available product sequences. Therefore, the need for a validation of those sequences for CBF measurements in specific neurovascular pathologies is demanded [9,10]. For cerebrovascular disease, only a few clinical validation studies have been conducted with product sequences[17–22]. Particularly for steno-occlusive disease, validation studies have not been performed for all available product sequences. Further, ASL in steno-occlusive disease is of high interest as it can be used in patients with contraindications for gadolinium and facilitates a noninvasive estimation of the cerebrovascular reactivity (CVR) [23]. In this respect, we aimed to define the performance of a commercially available ASL sequence (PICORE, pulsed ASL [PASL] technique) in patients with unilateral hemodynamically relevant steno-occlusive disease on a widely available 3T MRI system.

In PASL, the spins of protons of passing blood are inverted by a radiofrequency (RF)-pulse at a labeling slice usually at the neck,

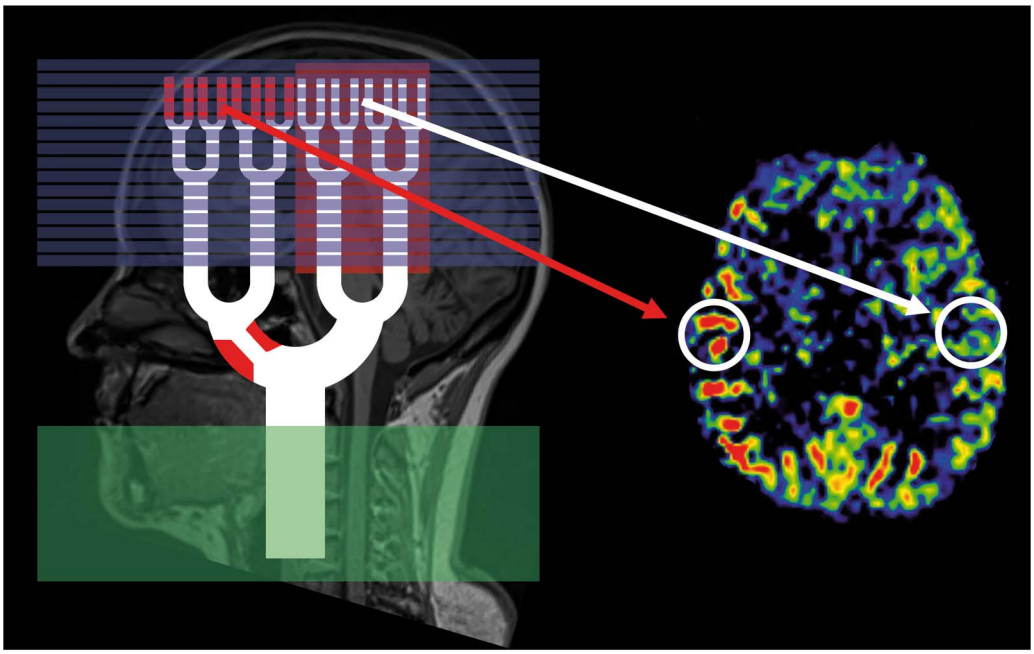

Figure 5. Arterial Transit Delay Artifact. Origin of the Arterial Transit Delay Artifact in ASL (labeling slice = green, imaging slices = blue). If arterial transit time is prolonged as it is the case in our patients, the inflow time is too short. Imaging slices capture high signal of labeled blood that is still in small arteries (as indicated by hyperintensities inside the labeling slices; red arrow) and hypointense areas, which the labeled blood has not yet reached. In parts of the brain where the arterial transit time is normal, blood has already exchanged with residual water and the ASL image appears normal (white arrow).
doi:10.1371/journal.pone.0087143.g005

covering the internal and external carotid and the vertebral arteries. By this technique, a single bolus of labeled blood is generated. The time this blood bolus needs to reach the brain capillaries is termed arterial transit time (ATT). In the brain capillary bed, labeled blood water then exchanges with residual tissue water. ASL images are acquired at one predefined time point after labeling, the inflow time (TI). It is important to notice that the TI has to be longer than the ATT to allow imaging in the capillary phase of blood transit. A second (control) image is then obtained without labeling. Subtraction of the two images yields perfusion weighted maps providing CBF-values. All ASL sequences in steno-occlusive disease, however, faces major obstacles owing to the prolonged ATT caused by stenosis/occlusion of brain feeding arteries. In this case, two signs may be observed: *First*, at the predefined inflow time, the blood bolus has not yet reached the capillary bed in the regions affected by steno-occlusion. Therefore, labeled blood is found mainly in precapillary arterioles. On ASL images, these vessels appear as hyperintense dots or lines depending on the image orientation [10,13,24]. *Second*, if the delay leads to very long arterial transit times, the blood bolus has not yet reached the perfusion territory at the predefined inflow time at all. In these regions, the signal is very low or lacks completely and thus severly underestimates real perfusion [10,25]. These signs represent the arterial transit delay artifact (ATDA) [10,13,24]. The origin of the ATDA is shown in figure 5, examples for both effects are shown in figure 6. Both effects may appear simultaneously when areas with different prolonged ATTs are present in one patient. Therefore, a patient with normal cerebral blood flow but delayed arrival time, might have a falsely elevated or a falsely decreased CBF in the ASL image (Figure 6). In line with pathophysiology, these effects were present in our study since ipsilateral ATDA was found in 12 of 17 patients (71%). On one hand, the presence of ATDAs clearly identified the site of DSC-TTP-delay and/or DSC-hypoperfusion in the qualitative analysis and areas with ATDA in ASL showed a longer median TTP-delay on TTP-maps. On the other hand, however, the hyperintense nature of ATDA led to an unreliable quantification of ASL-CBF. This causes a weak correlation between ASL-CBF and DSC CBF-values as indicated by BA-plot analysis. These results at 3 T are supported by previous results obtained at 1.5 T, Wolf et al. found no correlation between ASL-CBF and DSC-CBF at 1.5 T in patients with steno-occlusive disease [13]. In our ROI-based approach we chose large ROIs to account for spatial distortion of the different imaging modalities. As a consequence, our ROIs included white matter, in which ASL might not allow for reliable quantification of CBF. However, our volumetric analysis of gray matter perfusion alone did not lead to an improved correlation.

To account for the prolonged ATT in patients with steno-occlusive disease it would be possible to choose longer TIs [26], but most of the signal would be lost at that time [27]. This intrinsic problem can only be solved by multiple averaging but leads to unacceptable scanning times.

Out of 28, 11 data sets (39%) were uninterpretable owing to patient motion artifacts despite online motion correction (performed by 3D-PACE) and, generally, image quality in ASL was worse in comparison with DSC-MRI. Patients were asked to refrain from motion, and small pads were placed between the patient head and the coil to limit head movement. The high frequency of motion artifacts in our study - despite the mentioned measures, - might thus reflect a limitation of this method in our specific patient sample, as increased patient motion reflects clinical reality. This is supported by a validation of the same product sequence in acute stroke, where the authors also identified patient motion and imperfect motion correction as a major factor for limited image quality [18]. Offline motion correction by in-house

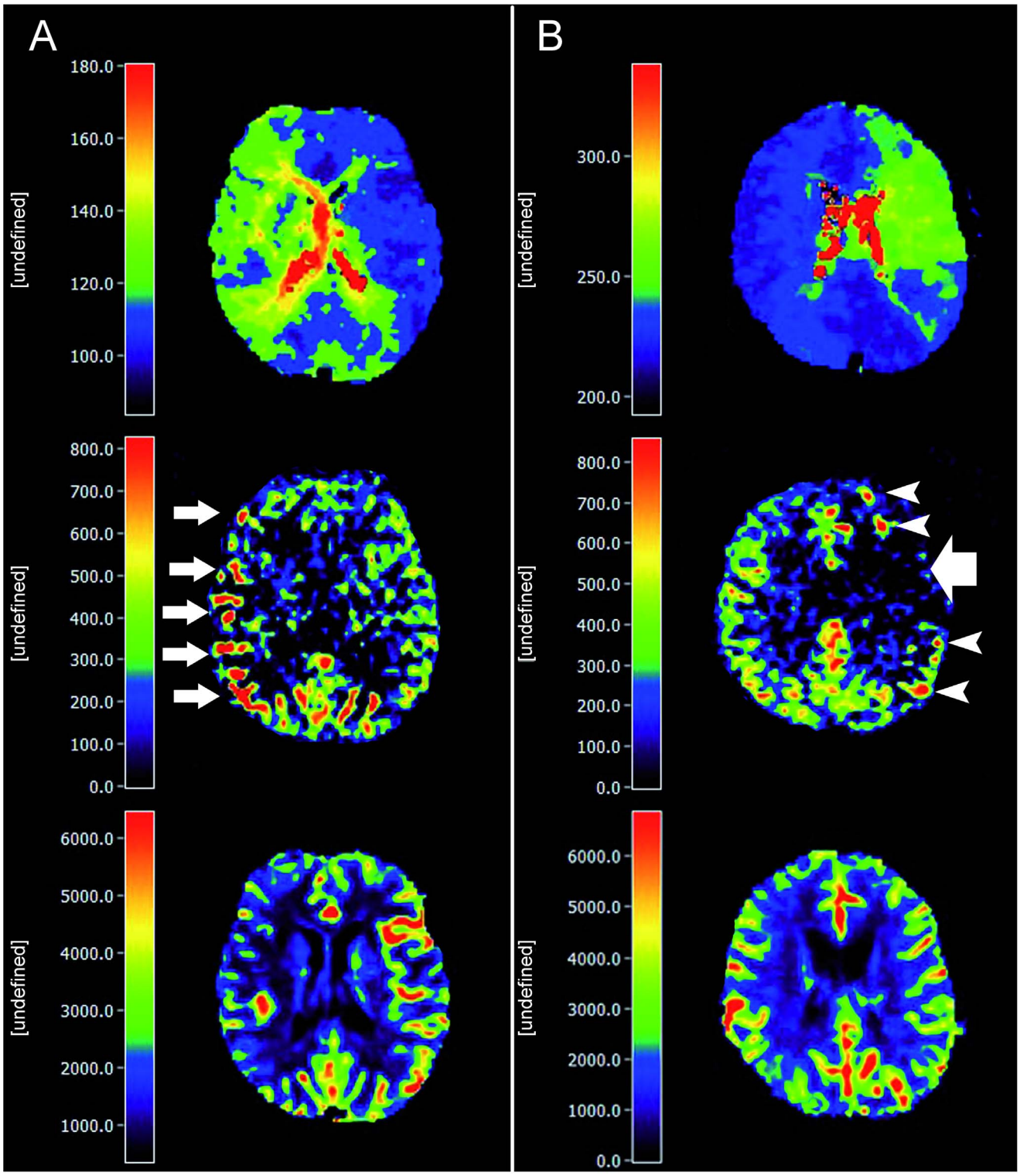

Figure 6. Exemplary patients showing blood arrival delay effects in ASL imaging. A) 66-year-old female, occlusion of the right ICA. The TTP image shows a visible ipsilateral delay (relTTP = 0.8 sec). In the ASL image, hyperintense arterial transit delay artifacts are seen (small white arrows). On the reference DSC-CBF map, a hypoperfusion in the affected hemisphere is present. B) 45-year-old female, occlusion of the left middle cerebral artery. In the ASL image, a hypointensity is seen in the area affected by delay (large white arrow, relTTP = 1.5 sec). In contrast, no apparent changes are present in the DSC-CBF map. In patient A, a moderate blood transit delay leads to the presence of hyperintense ADTA. The more severe delay in patient B might explain the hypointense ADTA surrounded by hyperintense areas in its borderzone as a sign of collateral macrovessels. All slices are coregistered. The scales do not represent absolute values.
doi:10.1371/journal.pone.0087143.g006

solutions might be preferable [28] but is not available in the clinical setting.

The described PICORE sequence offers the option of crusher gradients, that suppress intravascular blood signal [29] and reduce hyperintense vessel ATDAs. However, for reasons of methodology we did not choose this option: *First*, it does not eliminate the cause of the artifact, but its visibility. *Second*, the ATDA indicates the underlying transit delay and the lack of this information would render image analysis more difficult. *Third*, the use of crusher gradients further reduces the signal-to-noise ratio in ASL, which is already intrinsically low [10] especially in sequences without background suppression, e.g. the PICORE sequence.

Therefore, the PICORE product sequence available for the MRI system used in our study is not suited to reliably depict CBF in steno-occlusive disease at 3 T owing to the sensitivity to delayed blood arrival.

Currently, new ASL sequences address many methodological issues by correction for the delayed blood arrival time employing measurements at multiple inflow times. A very promising approach is a 3D ASL sequence (3D-GRASE) [30]. The benefit of this sequence in patients with steno-occlusive disease has been shown recently [31]. Another promising approach is the "look-locker approach" (ITS-FAIR [32], QUASAR [33]). Using this sequence in steno-occlusive disease at 3 T, recent studies found a high correlation with SPECT data [17] and a fair [34] to high [35] correlation with H2O-PET. These sequences, however, are not yet commercially available for all MRI systems.

Our study has some limitations: First, perfusion changes cannot be ruled out completely given the heterogeneity of perfusion alterations in patients with steno-occlusive disease. However, DSC-imaging followed ASL immediately and the clinical status of the measured patients was stable. Second, the methods of ASL and DSC differ considerably: While ASL uses blood as a freely diffusible and endogenous tracer, gadolinium in DSC mainly remains intravascular. Such methodological differences are a well-known difficulty of multimodal imaging and must be kept in mind when interpreting the results of comparative studies. While DSC-MRI can be considered a clinical standard for perfusion imaging, it is not a gold-standard. Methodological shortcomings include overemphasis of large vessels intrinsic to GRE-imaging [36] and the influence of the deconvolution method in patients with transit delay [37]. While a block circulant deconvolution (cSVD) might be preferable to sSVD from a technical point of view, this has been shown in direct comparison in only few pilot studies [37,38]. Additionally, cSVD requires much more computing power limiting its use in the clinical setting. Therefore, sSVD, as the current clinical standard, was chosen for the comparison with a clinically available ASL sequence in this study.

In conclusion, the commercially available ASL-sequence used in our study can indicate delay of blood arrival in steno-occlusive disease, but cannot be recommended for CBF measurement in these patients. New ASL-sequences present promising alternatives, but are not yet available for clinical use on all MRI systems.

Acknowledgments

We express our gratitude to the staff of the MRI unit at the Berlin Center for Advanced Neuroimaging (BCAN). We would like to thank especially Mrs. Andrea Hassenpflug for her excellent technical assistance.

Author Contributions

Conceived and designed the experiments: MM VM FS OZW MB JS. Performed the experiments: MM VM FS OZW SM KS SH JS. Analyzed the data: MM VM FS OZW GR MG JS. Contributed reagents/materials/analysis tools: MM VM FS OZW SH MG JS. Wrote the paper: MM VM FS JS.

References

1. Wintermark M, Sesay M, Barbier E, Borbély K, Dillon WP, et al. (2005) Comparative Overview of Brain Perfusion Imaging Techniques. Stroke 36: e83–e99. doi:10.1161/01.STR.0000177884.72657.8b.
2. Sobesky J (2012) Refining the mismatch concept in acute stroke: lessons learned from PET and MRI. J Cereb Blood Flow Metab 32: 1416–1425. doi:10.1038/jcbfm.2012.54.
3. Kaewlai R, Abujudeh H (2012) Nephrogenic systemic fibrosis. AJR Am J Roentgenol 199: W17–23. doi:10.2214/AJR.11.8144.
4. Levin JM, Kaufman MJ, Ross MH, Mendelson JH, Maas LC, et al. (1995) Sequential dynamic susceptibility contrast MR experiments in human brain: residual contrast agent effect, steady state, and hemodynamic perturbation. Magn Reson Med 34: 655–663.
5. Detre JA, Leigh JS, Williams DS, Koretsky AP (1992) Perfusion imaging. Magn Reson Med 23: 37–45.
6. Lehmann P, Monet P, de Marco G, Saliou G, Perrin M, et al. (2010) A comparative study of perfusion measurement in brain tumours at 3 Tesla MR: Arterial spin labeling versus dynamic susceptibility contrast-enhanced MRI. Eur Neurol 64: 21–26. doi:10.1159/000311520.
7. Lim YM, Cho YW, Shamim S, Solomon J, Birn R, et al. (2008) Usefulness of pulsed arterial spin labeling MR imaging in mesial temporal lobe epilepsy. Epilepsy Res 82: 183–189. doi:10.1016/j.eplepsyres.2008.08.001.
8. Donahue MJ, Strother MK, Hendrikse J (2012) Novel MRI approaches for assessing cerebral hemodynamics in ischemic cerebrovascular disease. Stroke 43: 903–915. doi:10.1161/STROKEAHA.111.635995.
9. Golay X, Guenther M (2012) Arterial spin labelling: final steps to make it a clinical reality. Magnetic Resonance Materials in Physics, Biology and Medicine 25: 79–82. doi:10.1007/s10334-012-0308-9.
10. Zaharchuk G (2012) Arterial Spin Labeling for Acute Stroke: Practical Considerations. Transl Stroke Res 3: 228–235. doi:10.1007/s12975-012-0159-8.
11. Luh W, Wong EC, Bandettini PA, Hyde JS (1999) QUIPSS II with thin-slice TI1 periodic saturation: A method for improving accuracy of quantitative perfusion imaging using pulsed arterial spin labeling. Magnetic Resonance in Medicine 41: 1246–1254. doi:10.1002/(SICI)1522–2594(199906)41:6<1246::AID-MRM22>3.0.CO;2-N.
12. Wong EC, Buxton RB, Frank LR (1998) Quantitative imaging of perfusion using a single subtraction (QUIPSS and QUIPSS II). Magn Reson Med 39: 702–708.
13. Wolf RL, Alsop DC, McGarvey ML, Maldjian JA, Wang J, et al. (2003) Susceptibility Contrast and Arterial Spin Labeled Perfusion MRI in Cerebrovascular Disease. Journal of Neuroimaging 13: 17–27. doi:10.1111/j.1552–6569.2003.tb00152.x.
14. Cízek J, Herholz K, Vollmar S, Schrader R, Klein J, et al. (2004) Fast and robust registration of PET and MR images of human brain. Neuroimage 22: 434–442. doi:10.1016/j.neuroimage.2004.01.016.
15. Tatu L, Moulin T, Vuillier F, Bogousslavsky J (2012) Arterial territories of the human brain. Front Neurol Neurosci 30: 99–110. doi:10.1159/000333602.
16. Detre JA, Rao H, Wang DJJ, Chen YF, Wang Z (2012) Applications of arterial spin labeled MRI in the brain. J Magn Reson Imaging 35: 1026–1037. doi:10.1002/jmri.23581.
17. Uchihashi Y, Hosoda K, Zimine I, Fujita A, Fujii M, et al. (2011) Clinical application of arterial spin-labeling MR imaging in patients with carotid stenosis: quantitative comparative study with single-photon emission CT. AJNR Am J Neuroradiol 32: 1545–1551. doi:10.3174/ajnr.A2525.
18. Huck S, Kerl HU, Al-Zghloul M, Groden C, Nölte I (2012) Arterial spin labeling at 3.0 Tesla in subacute ischemia: comparison to dynamic susceptibility perfusion. Clin Neuroradiol 22: 29–37. doi:10.1007/s00062-011-0126-x.
19. Zaharchuk G, Mogy ISE, Fischbein NJ, Albers GW (2012) Comparison of Arterial Spin Labeling and Bolus Perfusion-Weighted Imaging for Detecting Mismatch in Acute Stroke. Stroke 43: 1843–1848. doi:10.1161/STROKEAHA.111.639773.
20. Bivard A, Krishnamurthy V, Stanwell P, Levi C, Spratt NJ, et al. (2013) Arterial Spin Labeling Versus Bolus-Tracking Perfusion in Hyperacute Stroke. Stroke. doi:10.1161/STROKEAHA.113.003218.
21. Niibo T, Ohta H, Yonenaga K, Ikushima I, Miyata S, et al. (2013) Arterial spin-labeled perfusion imaging to predict mismatch in acute ischemic stroke. Stroke 44: 2601–2603. doi:10.1161/STROKEAHA.113.002097.
22. Huang YC, Liu HL, Lee JD, Yang JT, Weng HH, et al. (2013) Comparison of arterial spin labeling and dynamic susceptibility contrast perfusion MRI in patients with acute stroke. PLoS ONE 8: e69085. doi:10.1371/journal.-pone.0069085.
23. Bokkers RPH, van Osch MJP, van der Worp HB, de Borst GJ, Mali WPTM, et al. (2010) Symptomatic Carotid Artery Stenosis: Impairment of Cerebral Autoregulation Measured at the Brain Tissue Level with Arterial Spin-labeling MR Imaging. Radiology 256: 201–208. doi:10.1148/radiol.10091262.

24. Golay X, Hendrikse J, Lim TCC (2004) Perfusion imaging using arterial spin labeling. Top Magn Reson Imaging 15: 10–27.
25. Chng SM, Petersen ET, Zimine I, Sitoh YY, Lim CCT, et al. (2008) Territorial Arterial Spin Labeling in the Assessment of Collateral Circulation Comparison With Digital Subtraction Angiography. Stroke 39: 3248–3254. doi:10.1161/STROKEAHA.108.520593.
26. Alsop DC, Detre JA (1996) Reduced transit-time sensitivity in noninvasive magnetic resonance imaging of human cerebral blood flow. J Cereb Blood Flow Metab 16: 1236–1249. doi:10.1097/00004647–199611000–00019.
27. Qiu D, Straka M, Zun Z, Bammer R, Moseley ME, et al. (2012) CBF measurements using multidelay pseudocontinuous and velocity-selective arterial spin labeling in patients with long arterial transit delays: Comparison with xenon CT CBF. Journal of Magnetic Resonance Imaging 36: 110–119. doi:10.1002/jmri.23613.
28. Bivard A, Stanwell P, Levi C, Parsons M (2013) Arterial spin labeling identifies tissue salvage and good clinical recovery after acute ischemic stroke. J Neuroimaging 23: 391–396. doi:10.1111/j.1552–6569.2012.00728.x.
29. Ye FQ, Mattay VS, Jezzard P, Frank JA, Weinberger DR, et al. (1997) Correction for vascular artifacts in cerebral blood flow values measured by using arterial spin tagging techniques. Magn Reson Med 37: 226–235.
30. Günther M, Oshio K, Feinberg DA (2005) Single-shot 3D imaging techniques improve arterial spin labeling perfusion measurements. Magnetic Resonance in Medicine 54: 491–498. doi:10.1002/mrm.20580.
31. MacIntosh BJ, Lindsay AC, Kylintireas I, Kuker W, Günther M, et al. (2010) Multiple inflow pulsed arterial spin-labeling reveals delays in the arterial arrival time in minor stroke and transient ischemic attack. AJNR Am J Neuroradiol 31: 1892–1894. doi:10.3174/ajnr.A2008.
32. Günther M, Bock M, Schad LR (2001) Arterial spin labeling in combination with a look-locker sampling strategy: inflow turbo-sampling EPI-FAIR (ITS-FAIR). Magn Reson Med 46: 974–984.
33. Petersen ET, Lim T, Golay X (2006) Model-free arterial spin labeling quantification approach for perfusion MRI. Magn Reson Med 55: 219–232. doi:10.1002/mrm.20784.
34. Bokkers RP, Bremmer JP, van Berckel BN, Lammertsma AA, Hendrikse J, et al. (2009) Arterial spin labeling perfusion MRI at multiple delay times: a correlative study with H215O positron emission tomography in patients with symptomatic carotid artery occlusion. J Cereb Blood Flow Metab 30: 222–229.
35. Kamano H, Yoshiura T, Hiwatashi A, Abe K, Togao O, et al. (2013) Arterial spin labeling in patients with chronic cerebral artery steno-occlusive disease: correlation with (15)O-PET. Acta Radiol 54: 99–106. doi:10.1258/ar.2012.120450.
36. Boxerman JL, Hamberg LM, Rosen BR, Weisskoff RM (1995) MR contrast due to intravascular magnetic susceptibility perturbations. Magn Reson Med 34: 555–566.
37. Wu O, Østergaard L, Weisskoff RM, Benner T, Rosen BR, et al. (2003) Tracer arrival timing-insensitive technique for estimating flow in MR perfusion-weighted imaging using singular value decomposition with a block-circulant deconvolution matrix. Magn Reson Med 50: 164–174. doi:10.1002/mrm.10522.
38. Matsushima S, Kubota T, Yamada K, Akazawa K, Masunami T, et al. (2008) Effect of vascular stenosis on perfusion-weighted imaging; differences between calculation algorithms. J Magn Reson Imaging 27: 1103–1108. doi:10.1002/jmri.21362.

3D GRASE pulsed arterial spin labeling at multiple inflow times in patients with long arterial transit times: comparison with dynamic susceptibility-weighted contrast-enhanced MRI at 3 Tesla

Steve Z. Martin, Vince I. Madai, Federico C. von Samson-Himmelstjerna, Matthias A. Mutke, Miriam Bauer, Cornelius X. Herzig, Stefan Hetzer, Matthias Günther and Jan Sobesky.

Journal of Cerebral Blood Flow & Metabolism, 2015
Mar;35(3):392-401. Epub 2014 Nov 19.

https://dx.doi.org/10.1038/jcbfm.2014.200

OPEN ACCESS Freely available online

PLOS ONE

DWI Intensity Values Predict FLAIR Lesions in Acute Ischemic Stroke

Vince I. Madai[1,5], Ivana Galinovic[1], Ulrike Grittner[1,6], Olivier Zaro-Weber[1,2], Alice Schneider[1,6], Steve Z. Martin[1], Federico C. v. Samson-Himmelstjerna[1,3], Katharina L. Stengl[1,5], Matthias A. Mutke[1,5], Walter Moeller-Hartmann[4], Martin Ebinger[1,5], Jochen B. Fiebach[1], Jan Sobesky[1,5]*

1 Center for Stroke Research Berlin (CSB), Charité-Universitätsmedizin, Berlin, Germany, **2** Max-Planck-Institute for Neurological Research, Cologne, Germany, **3** Fraunhofer MEVIS, Bremen, Germany, **4** Department of Radiology, Krankenhaus Ludmillenstift, Meppen, Germany, **5** Department of Neurology, Charité-Universtitätsmedizin, Berlin, Germany, **6** Department for Biostatistics and Clinical Epidemiology, Charité-Universitätsmedizin, Berlin, Germany

Abstract

Background and Purpose: In acute stroke, the DWI-FLAIR mismatch allows for the allocation of patients to the thrombolysis window (<4.5 hours). FLAIR-lesions, however, may be challenging to assess. In comparison, DWI may be a useful bio-marker owing to high lesion contrast. We investigated the performance of a relative DWI signal intensity (rSI) threshold to predict the presence of FLAIR-lesions in acute stroke and analyzed its association with time-from-stroke-onset.

Methods: In a retrospective, dual-center MR-imaging study we included patients with acute stroke and time-from-stroke-onset ≤12 hours (group A: n = 49, 1.5T; group B: n = 48, 3T). DW- and FLAIR-images were coregistered. The largest lesion extent in DWI defined the slice for further analysis. FLAIR-lesions were identified by 3 raters, delineated as regions-of-interest (ROIs) and copied on the DW-images. Circular ROIs were placed within the DWI-lesion and labeled according to the FLAIR-pattern (FLAIR+ or FLAIR−). ROI-values were normalized to the unaffected hemisphere. Adjusted and nonadjusted receiver-operating-characteristics (ROC) curve analysis on patient level was performed to analyze the ability of a DWI- and ADC-rSI threshold to predict the presence of FLAIR-lesions. Spearman correlation and adjusted linear regression analysis was performed to assess the relationship between DWI-intensity and time-from-stroke-onset.

Results: DWI-rSI performed well in predicting lesions in FLAIR-imaging (mean area under the curve (AUC): group A: 0.84; group B: 0.85). An optimal mean DWI-rSI threshold was identified (A: 162%; B: 161%). ADC-maps performed worse (mean AUC: A: 0.58; B: 0.77). Adjusted regression models confirmed the superior performance of DWI-rSI. Correlation coefficents and linear regression showed a good association with time-from-stroke-onset for DWI-rSI, but not for ADC-rSI.

Conclusion: An easily assessable DWI-rSI threshold identifies the presence of lesions in FLAIR-imaging with good accuracy and is associated with time-from-stroke-onset in acute stroke. This finding underlines the potential of a DWI-rSI threshold as a marker of lesion age.

Citation: Madai VI, Galinovic I, Grittner U, Zaro-Weber O, Schneider A, et al. (2014) DWI Intensity Values Predict FLAIR Lesions in Acute Ischemic Stroke. PLoS ONE 9(3): e92295. doi:10.1371/journal.pone.0092295

Editor: Jean-Claude Baron, INSERM U894, Centre de Psychiatrie et Neurosciences, Hopital Sainte-Anne and Université Paris 5, France

Received June 20, 2013; **Accepted** February 21, 2014; **Published** March 21, 2014

Funding: The research leading to these results has received funding from the German Federal Ministry of Education and Research via the grant "Center for Stroke Research Berlin" (01 EO 0801; http://www.bmbf.de). The funders had no role in study design, data collection and analysis, decision to publish, or preparation of the manuscript.

Competing Interests: The authors have read the journal's policy and make the following disclosures: JBF reports the following board memberships, consultancies and/or payments for lectures including service on speakers bureaus: Boehringer-Ingelheim, Lundbeck, Siemens, Sygnis, and Synarc. JS reports the following board memberships, consultancies and/or payments for lectures including service on speakers bureaus: Boehringer-Ingelheim, Bayer, Pfizer and Maquet. There are no patents, products in development or marketed products to declare. This does not alter the authors' adherence to all the PLOS ONE policies on sharing data and materials.

* E-mail: jan.sobesky@charite.de

Introduction

In patients with acute ischemic stroke, the combination of a hyperintense lesion in diffusion weighted imaging (DWI) and the absence of a corresponding lesion in T2-weighted fluid-attenuated inversion recovery (FLAIR) imaging, the so called DWI-FLAIR mismatch, can predict the time from stroke onset <4.5 h [1]. This can be attributed to the time-dependent appearance of FLAIR-lesions within the first hours after stroke onset [2–4]. This finding is promising, as identification of patients eligible for thrombolysis with unknown stroke onset, e.g. in wake-up stroke, may be facilitated by specific imaging markers. However, the visual assessment of FLAIR lesions may be difficult [5,6] and the automated analysis of FLAIR images is challenging owing to low contrast and partial volume effects [7]. Lesions on DW-images, on the other hand, show high contrast and can be easily delineated by automated software solutions [8] making DWI suitable for clinical stroke trials. In the present work, we hypothesized that DWI signal-intensity increases with the time-from-stroke-onset. To test this hypothesis we investigated, whether relative DWI intensity

(DWI-rSI) is associated a) with the presence of hyperintensities in FLAIR-imaging and b) with time-from-stroke-onset.

Materials and Methods

Ethics Statement

All patients gave informed written consent prior to the study. The study was conducted according to the principles expressed in the Declaration of Helsinki and was approved by the authorized institutional review boards (IRB) of the University of Cologne and the Charité-Universitätsmedizin Berlin.

Study Design

We performed a dual center retrospective observational imaging study. Imaging data including DW- and FLAIR-images were acquired from two stroke imaging databases: Group A, 1.5 T MR-imaging, University of Cologne, neurological imaging data base. Stroke patients available for the analysis were imaged consecutively between 2/2002 and 5/2004, in total 430 patients; Group B, 3 T MR-imaging, Charité-Universitätsmedizin Berlin, stroke imaging data base. Stroke patients available for the analysis were imaged consecutively between 3/2008 and 8/2010, in total 347 patients. Databases were screened and patients were included according to the following criteria: 1) clinically proven stroke, 2) confirmed symptom onset <12 h, 3) confirmed unilateral stroke lesion in DW-imaging, 4) available FLAIR imaging. Exclusion criteria were: 1) insufficient image quality, 2) incomplete clinical data, 3) punctate lesions and 4) brainstem infarctions. For a flow chart depicting the exclusions from the individual databases, see figure 1.

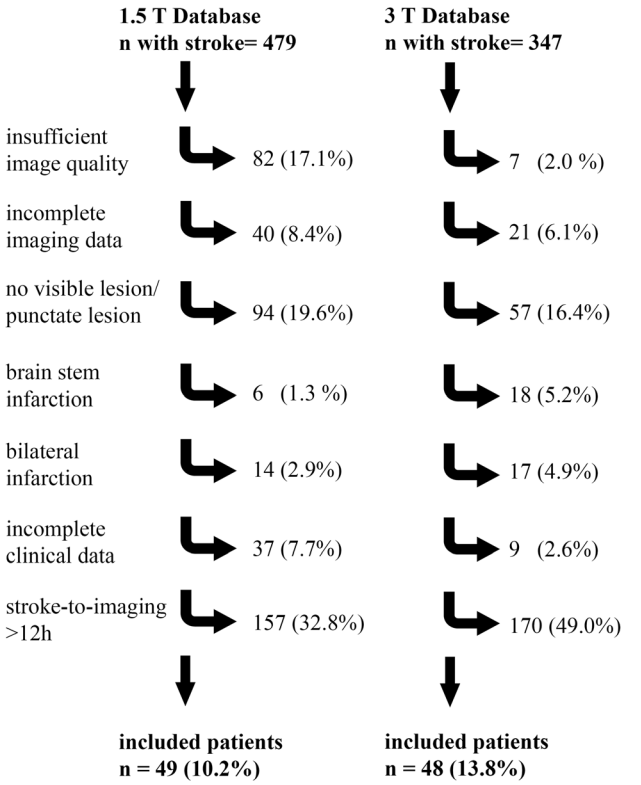

Figure 1. Database screening results and final study inclusion rate. In both databases the exclusion criterion with the highest exclusion rate was a stroke-to-imaging-time higher than 12 hours. In the 1.5 T database, the number of patients, which had to be excluded due to insufficient image quality (mainly of FLAIR images), was much higher (17.1%) than in the 3 T database (2.0%).
doi:10.1371/journal.pone.0092295.g001

Magnetic Resonance Imaging Hardware

MR-imaging was performed at 1.5 T on a Philips Gyroscan Intera Master whole-body system (Philips Medical Systems, Best, The Netherlands). At 3 T, a Magnetom Tim Trio whole-body system (Siemens Healthcare, Erlangen, Germany) was used.

Magnetic Resonance Imaging Parameters

DW- and FLAIR imaging parameters were:

- At 1.5 T:
    - DWI: single shot SE-EPI (TE: 96 ms, TR: 3560 ms, flip angle: 90°, matrix: 256×256, FoV: 230×230, b:0 and b:1000, pixel size: 0.9×0.9 mm^2, slice thickness: 6 mm, interslice gap: 0.6 mm)
    - T2-weighted FLAIR: (TE: 100 ms, TR: 6000 ms, TI: 2000 ms, flip angle: 90°, matrix: 256×256, FoV: 220×220, pixel size 0.9×0.9 mm^2, slice thickness: 6 mm, interslice gap: 0.6 mm)
- At 3 T:
    - DWI: single shot SE-EPI (TE: 93 ms, TR: 7600 ms, flip angle: 90°, matrix: 192×192, FoV: 230×230, b:0 and b:1000, pixel size 1.2×1.2 mm^2, slice thickness: 2.5 mm)
    - T2-weighted FLAIR: (TE: 100 ms, TR: 8000 ms, TI: 2370 ms, flip angle: 130°, matrix: 256×256, FoV: 220×220, pixel size 0.9×0.9 mm^2, slice thickness: 5 mm, interslice gap: 0.5 mm).

Data Postprocessing and Image Analysis

Co-registration and post-processing of DW- and FLAIR images was performed with VINCI, Version 2.63 (Max-Planck-Institute for Neurological Research, Cologne, Germany) [9]. DWI lesion volumina were assessed using MRIcron (Chris Rorden, http://www.mccauslandcenter.sc.edu/mricro/). At 3 T, DW images were resized in the z-axis to match FLAIR images.

In DWI, the slice with the largest lesion extent was identified visually and used for the complete further analysis. DW-images were co-registered to FLAIR images and the absence or presence of FLAIR lesions was assessed by three raters blinded to clinical data and DW-images (experience in stroke imaging is indicated for each rater; Rater 1, VIM: 3 years, Rater 2, ME: 5 years, Rater 3, JS: 10 years). Prior to the rating, raters were encouraged to look for subtle intensity changes by adjusting contrast and brightness of the images and to compare intensities of potentially hyperintense regions with the healthy contralateral hemisphere. Such subtle intensity changes were also rated as a FLAIR hyperintensity. The area of the FLAIR lesion was individually delineated by each rater and copied on the DW-images. Then, 6 mm regions of interest (ROIs) were placed within the whole DWI-lesion. Each ROI was labeled according to its position in regard to the FLAIR-ROI. If it was located inside the FLAIR lesion, it was labeled FLAIR+ (positive), if it was located outside of the FLAIR lesion, it was labeled as FLAIR- (negative). If a FLAIR lesion was absent, all DWI ROIs of this patient were labeled as FLAIR-. For a graphical overview of the analysis see figure 2. ROI-values were normalized

as a ratio: [100% x (mean ROI value/mean value of the unaffected hemisphere)], taken from a slice at the height of the lateral ventricles and above the putamen encompassing the corona radiata. In cases of cerebellar infarction, a ROI of the contralateral cerebellar hemisphere was used to normalize the ROI values. Above steps were performed equally for apparent diffusion coefficient (ADC)-maps.

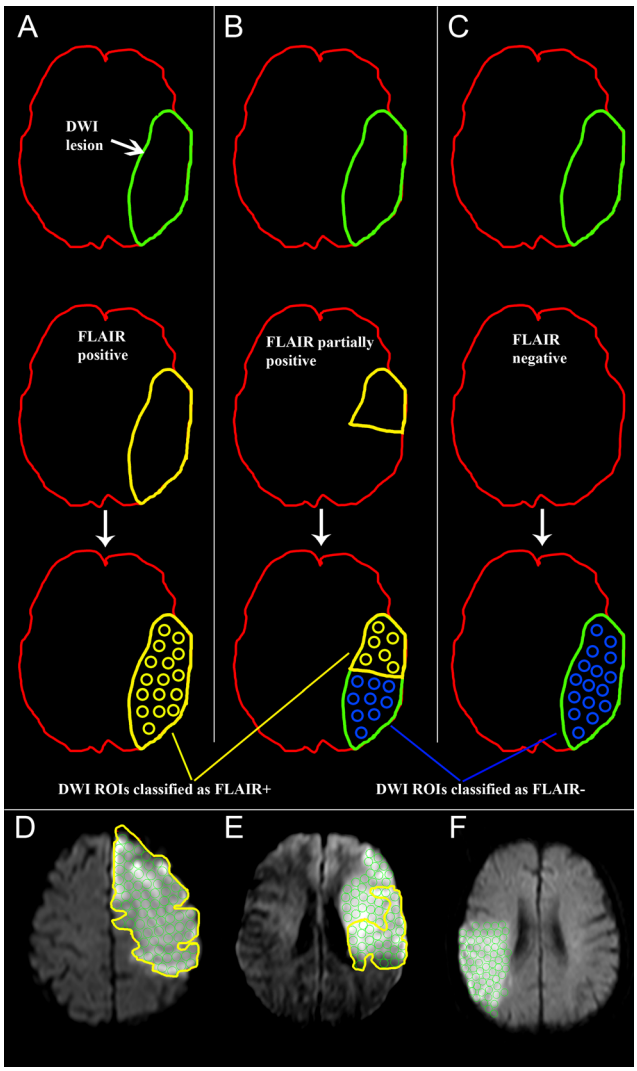

Figure 2. Labeling of lesions in DWI imaging according to the FLAIR pattern. A) In case of a FLAIR lesion encompassing the whole DWI-lesion, the hyperintensity was delineated as a region of interest (ROI) (A, second row). The FLAIR-ROI was then copied on the DWI and filled with 6 mm circular ROIs (A, third row)). These ROIs were classified as FLAIR+. B) In cases, in which the FLAIR-ROI did not completely match the DWI-lesion (B, second row), ROIs inside the FLAIR-ROI were classified as FLAIR+, and those outside as FLAIR- (B, third row). C) If no FLAIR lesion was identified (C, second row), the whole DWI lesion was filled with circular ROIs, which were classified as FLAIR- (C, third row). These steps were performed equally in ADC-maps. D), E) and F) show examples in analogy to the scheme, D) showing a patient, where the delineated FLAIR-ROI encompasses the whole DWI-lesion, E) depicting a patient, where the FLAIR-lesion only partially covers the DWI-lesion. Lastly, F) shows a patient, where all DWI-ROIs were labelled as FLAIR- in the absence of a visible FLAIR lesion.
doi:10.1371/journal.pone.0092295.g002

Statistical Analysis

Owing to skewed distribution of some variables, results are presented as median and interquartile range (IQR) if not indicated otherwise. Differences in clinical data between groups were assessed using the Mann-Whitney U rank sum test.

Agreement between raters for the identification of FLAIR-hyperintensities was analyzed using free-marginal kappa [10,11]. Kappa values were evaluated as suggested by Landis and Koch [12].

ROI-analysis was performed on patient level and separately for the two centres. We used mean ROI-values per patient and per rater for positive ROIs and negative ROIs separately:

a) If all raters had some ROIs of a patient classified as having a positive FLAIR status, we used only the mean of the positive values and classified the patient as having a positive flair status.

b) If not all raters found positive ROIs for a patient, but all raters had ROIs classified as negative, we used only the mean of the negative ROI-values and classified the patient as negative. *

c) Only for some patients one of the raters classified all ROIs in another category as the other raters. For them we used the classification of the two corresponding raters and set the ROI value for the rater not corresponding to missing.

In the next step, the ability of a relative DWI-intensity threshold to predict the presence of corresponding FLAIR-hyperintensities was analyzed using an unadjusted receiver operating characteristics (ROC) curve analysis. The area under the curve (AUC) and the 95% confidence limits for the raters are reported. To get the optimal threshold, the Youden Index was used ([13]. Sensitivity, specificity, and predictive values for the optimal thresholds are also reported.

To adjust for possible confounders, a multiple logistic regression model with the dependent variable "FLAIR-status" and independent variables "lesion volume", "sex", "thrombolysis" and "NIHSS" was used as a basic model (m0). In the additional model 1 (m1), "age" was added. Finally, different models were compared with regard to their ability to discriminate individuals in their FLAIR-status:

i) In model 2 (m2), we added "time-from-stroke-onset" to the m1 model.

ii) In model 3 (m3), we added the ROI-intensity for each rater separately to the m1 model. Paired sample statistical techniques were used for the comparison of two models. The method exploits the mathematical equivalence of the AUC to the Mann-Whitney U-statistic [14]. The ROC curves were calculated using SPSS Statistics 21, Release Version 21.0.0.0 (SPSS, Inc., 2012, Chicago, IL, www.spss.com). The comparisons of ROC curves and the linear mixed models were done using SAS software, Version 9.3 of the SAS System for Windows. (2010 SAS Institute Inc., Cary, NC, USA).

For analyzing the association between DWI-rSI and time-from-stroke-onset we calculated the mean DWI intensity over all ROIs and raters for every patient and used unadjusted and adjusted correlation analysis (Spearman's rank correlation) and a multiple linear regression analysis adjusted for "age", "lesion volume" and "thrombolysis". We calculated multiple linear regressions with (log-transformed) "mean DWI-value" as dependent variable and "age", "thrombolysis" and (log-transformed) "lesion volume" as independent variables. Mean DWI intensities and lesion volume values were log-transformed to overcome the skewness in the distribution of the values. We analyzed the adjusted association between mean DWI-rSI and time-from-stroke-onset by analyzing the association of the residuals from the regression analysis with time-from-stroke-onset.

Above steps were performed equally for ADC-maps.

Results

In group A (1.5 T), 49 patients (16 females) and in group B (3 T) 48 patients (22 females) were included in the analysis. Median values for clinical data were (Group A/Group B): Time-from-stroke-onset (h) was 2.4/2.0; age (years) was 62/74; NIHSS (points) was 8/5 and the lesion volume (ml) was 22.9/6.8. The two groups differed significantly in age, NIHSS and lesion volume, but not in the time-from-stroke-onset. Five patients had cerebellar infarction (1 in group A and 4 in group B). Detailed patient data are shown in Table 1.

Interrater agreement for the rating of FLAIR images as positive or negative for hyperintensities was substantial for both group A and group B with a kappa value of 0.62/0.69 (overall agreement was 81%/85%).

In the unadjusted ROC curve analysis, relative DWI-intensities performed well in discriminating hyperintensities in FLAIR imaging in both groups and for all 3 raters (results for groups and 3 raters; Group A: AUC 0.84, 0.91, 0.76 [mean: 0.84]; Group B: AUC 0.87, 0.86, 0.83 [mean: 0.85]). The Youden-Index identified comparable optimal relative DWI-intensity thresholds for both groups for all 3 raters (in %; Group A: 162, 158, 167, mean: 162; Group B: 163, 161, 159, mean: 161). In contrast, relative ADC-intensity values performed worse (group A: AUC 0.56, 0.55, 0.64; group B: AUC 0.74, 0.80, 0.77). Detailed data including sensitivity, specificity, positive and negative predictive value for the identified thresholds are listed in Table 2.

Table 1. Clinical data, imaging data and comparison of patient groups.

	Group A (1.5 T)	Group B (3 T)	p
Patients (n)	49	48	
Time Stroke to Imaging (h)	2.4 (1.7–5.3)	2.0 (1.0–3.7)	0.115
Age (y)	62 (52–67)	74 (64–84)	<0.001*
NIHSS (points)	8 (6–13)	5 (4–13)	0.047*
Stroke lesion volume (mm3)	22.9 (9.2–45.1)	6.8 (2.5–21.4)	<0.001*
Imaging time window after stroke			
0–4.5 h	34 (69.4%)	39 (81.3%)	
4.6–6 h	4 (8.2%)	3 (6.3%)	
6.1–12 h	11 (22.4%)	6 (12.5%)	
Thrombolysis rate	25 (51%)	26 (54.2%)	
Acute visible vessel occlusion[a]	21 (42.9%)	27 (56.3%)	
ACA	0	5	
MCA	13	22	
PCA	1	1	
ICA/CCA	7	1	
VA/BA	1	2	
Lesion location			
ACA-territory	1 (2.0%)	1 (2.1%)	
MCA-territory	45 (91.8%)	39 (81.3%)	
PCA-territory	2 (4.1%)	4 (8.3%)	
Cerebellum	1 (2.0%)	4 (8.3%)	

Data are given as median and IQR (interquartile range); Groups were compared using the Mann-Whitney U rank sum test, significant differences are marked by an asterisk; n, number; h, hours; y, years; ACA: anterior cerebral artery; MCA: middle cerebral artery; PCA: posterior cerebral artery; ICA/CCA: internal/common carotid artery; VA: vertebral artery; BA: basilar artery. [a] = if patients had occlusion in two different vessels at the same time (e.g. ICA and MCA), occlusion was indicated for both vessels.
doi:10.1371/journal.pone.0092295.t001

In the adjusted ROC-analysis for DWI, the basic model m0 including "lesion volume", "sex", "thrombolysis" and "NIHSS" had only a weak discrimination value for FLAIR status (AUC; Group A = 0.65; Group B = 0.59). The m1 model, where information on "age" was added, had a higher discrimination value (AUC; Group A = 0.73; Group B = 0.78). Adding "time-from-stroke-onset" to model m1 led to a further (significant) increase of the discrimination (model 2; AUC; Group A = 0.87; Group B = 0.91). Adding the ROI values for each rater as a variable in the m1-model, the increase was also significant in comparison with the m1 model and the discrimination value was comparable to the model 2 (model 3; mean AUC; Group A: 0.93; Group B: 0.93). Detailed data including p-values for the model comparison are listed in table 3. ROC-curves for model m0, m1, m2 and m3 for each rater are shown in figure 3.

For ADC in contrast, adding of ROI values in the m3 model did not increase the discrimination value. On the contrary, model 3 performed even worse than model 2, which was based on "time-from-stroke-onset". Detailed data including p-values for the model comparison are listed in table 4. ROC-curves for model m0, m1, m2 and m3 for each rater are shown in figure 3.

In the unadjusted correlation analysis, a significant moderate to good correlation between mean relative DWI intensity and time-from-stroke-onset was found (Group A: $r_s = 0.54$ ($p<0.001$); Group B: $r_s = 0.73$ ($p<0.011$). The adjusted correlation confirmed a moderate to good correlation (Group A: $r_s = 0.45$ ($p<0.001$;, Group B: $r_s = 0.69$ ($p<0.011$) with a significant moderate fit in the linear regression analysis (see figure 4).

For ADC in contrast, no correlation was found between ADC and time-frome-stroke-onset (unadjusted analysis: Group A $r_s = -0.25$, Group B $r_s = 0.07$; adjusted analysis: Group A $r_s = -0.22$, Group B $r_s = 0.05$) and no fit was present in the linear regression analysis (see figure 4).

Discussion

We report on the ability of a relative DWI-intensity threshold to discriminate with good accuracy between absence or presence of hyperintensities in corresponding FLAIR-images at both 1.5 and 3 T. The presence of FLAIR-hyperintensities was determined by 3 readers, who showed substantial interrater agreement. At both field strengths, similar DWI-intensity thresholds were identified. In addition, DWI intensity showed a significant association with time-from-stroke-onset.

To date, patients with unknown time from stroke onset are excluded from intravenous thrombolysis [15,16]. As stroke incidence rates are higher in the morning hours compared to the rest of the day [17], patients *in theory* eligible for thrombolysis are *in practice* excluded from thrombolysis if time of stroke onset is unknown. Strategies to identify patients eligible for thrombolysis by MRI have been a major focus of interest in stroke research [18]. While ischemic lesions are visible in DWI as early as several minutes after stroke [19], lesions in T2-weighted FLAIR imaging show a later appearance, where the majority of patients displays FLAIR lesions only after several hours of stroke [2][3][4]. Thus, it is not surprising that the DWI-FLAIR mismatch allows for the allocation of patients to the current thrombolysis time window (i.e. <4.5 h after stroke) with a high specificity and a high positive predictive value [1]. The use of the DWI-FLAIR mismatch, however, mainly relies on the visual assessment of FLAIR hyperintensities. On one hand, visual qualitative assessment of FLAIR-images is challenging [6]. On the other hand, an

Table 2. Detailed results of the unadjusted ROC analysis for all 3 raters at 1.5 and 3 T.

	AUC (95%CI)	Threshold (%)	Sensitivity (%)	Specificity (%)	PPV (%)	NPV (%)
1.5 T DWI						
Rater 1 (n = 49)	0.84(0.72–0.95)	162	63.0	95.5	94.4	67.7
Rater 2 (n = 47)	0.91(0.84–0.99)	158	80.0	86.4	87.0	79.2
Rater 3 (n = 49)	0.76(0.63–0.89)	167	44.4	100.0	100.0	59.5
mean	0.84	162	62.5	93.7	93.8	68.8
3 T DWI						
Rater 1 (n = 48)	0.87 (0.77–0.89)	163	80.0	82.6	83.3	79.2
Rater 2 (n = 47)	0.86 (0.76–0.97)	161	79.2	78.3	79.2	78.3
Rater 3 (n = 46)	0.83 (0.71–0.95)	159	78.3	78.3	78.3	78.3
mean	0.85	161	79.2	79.7	80.3	78.6
1.5 T ADC						
Rater 1 (n = 49)	0.56 (0.40–0.73)	64	70.4	45.5	61.3	55.6
Rater 2 (n = 48)	0.55 (0.38–0.71)	69	53.8	68.2	66.7	55.6
Rater 3 (n = 49)	0.64 (0.49–0.80)	78	44.4	90.9	85.7	57.1
mean	0.58	70	56,2	68,2	71,2	56,1
3 T ADC						
Rater 1 (n = 48)	0.74 (0.59–0.88)	65	48.0	100.0	100.0	63.9
Rater 2 (n = 47)	0.80 (0.67–0.94)	60	70.8	87.0	85.0	74.1
Rater 3 (n = 46)	0.77 (0.62–0.91)	61	69.6	87.0	84.2	74.1
mean	0.77	62	62,8	91,3	89,7	70,7

At both 1.5 and 3 T, the ability of a relative DWI- or ADC threshold to predict the presence of lesion in FLAIR-imaging was investigated individually for 3 raters. The given threshold is the optimal relative intensity value cutoff determined by the Youden-Index. For each threshold, the corresponding sensitivity, specificity, PPV and NPV and their means are shown. 95% confidence intervals are given for each individual AUC. DWI-rSI performed better in discriminating hyperintensities in FLAIR imaging than ADC-rSI. AUC, Area under the curve; PPV, positive predictive value; NPV, negative predictive value.

doi:10.1371/journal.pone.0092295.t002

automated analysis and the delineation of lesions in FLAIR imaging may be difficult owing to low contrast and partial volume effects [7]. This explains, why the use of quantitative relative FLAIR-intensity values has led to heterogenous results [3][4][20][21]. We therefore hypothesized that DWI-maps might yield a surrogate of FLAIR imaging and we were able to show that a DWI based threshold predicts the presence of a FLAIR lesion with good performance across two different MR field strengths and three independent raters. In addition, mean DWI intensity of the lesion showed significant association with time-from-stroke-onset. These results strongly indicate two important points: *First*, DWI-intensity might exhibit a time-dependent increase after onset of ischemia in the acute phase. This specifies previous findings by Petkova et al. that described different DWI intensity values in patient samples stratified according to time-from-stroke-onset [4]. In that work, DWI-rSI was able to allocate patients to the thrombolysis time window <3 h (AUC: 0.75), but did not perform better than ADC-rSI (AUC: 0.74). It should be noted, however, that the authors projected the DWI lesion as a mask on ADC-maps and did not delineate the lesion in ADC-maps individually to derive rSI values. The reported threshold for DWI for the allocation of patients to the thrombolysis window was 19% using the formula "(DWI-lesion - contralateral value)/(DWI-lesion + contralateral value) × 100". Recalculating our threshold of 160% rSI according to that formula leads to a similar threshold of 23% corroborating the pivotal association between FLAIR-appearance, DWI-rSI and time-from-stroke-onset.

Second, our results indicate that DWI-intensity is associated with tissue fate. The finding that a DWI-intensity threshold allows the prediction of FLAIR hyperintensity suggests that DWI-intensity follows a pathophysiologically driven time course similar to the manifestation of FLAIR lesions rather than simply increasing linearly with time. This is corroborated by previous results showing that a certain DWI-intensity threshold (118%) was able to predict permanent infarction as shown in an acute stroke sample imaged by MRI and comparative positron emission tomography [22]. This is important, as the DWI/FLAIR mismatch is limited by a high percentage of patients showing FLAIR positive lesion early after stroke [1]. Recently, it has been reported that this is even more pronounced at 3T, where a high percentage of patients showed FLAIR hyperintensities within the thrombolysis time window (44.5%) [23]. In this context, biomarkers are of interest, which are linked to tissue fate [3] and DWI intensity might serve this purpose.

It should be noted, that our analysis is an explorative and hypothesis-generating imaging study, in which only one representative slice per patient was analyzed. Based on our findings, it will be of major clinical interest to establish the relationship of DWI-intensity values and time-from-stroke-onset and tissue fate by analyzing the whole DWI lesion volume in future studies. Using such an approach, also the allocation to the 4.5 hours thrombolysis time window by DWI intensity can be investigated.

Our results rely in part on the assessment of FLAIR images as "positive" or "negative". The raters were encouraged to look for even subtle changes by adjusting contrast and brightness and by comparing the putative lesion intensity with the intensity of the contralateral hemisphere. Following this predefined algorithm, a substantial agreement as measured by interrater kappa could be achieved. However, in this clinically relevant technique, overall agreement did not exceed 85%. This finding corroborates that the

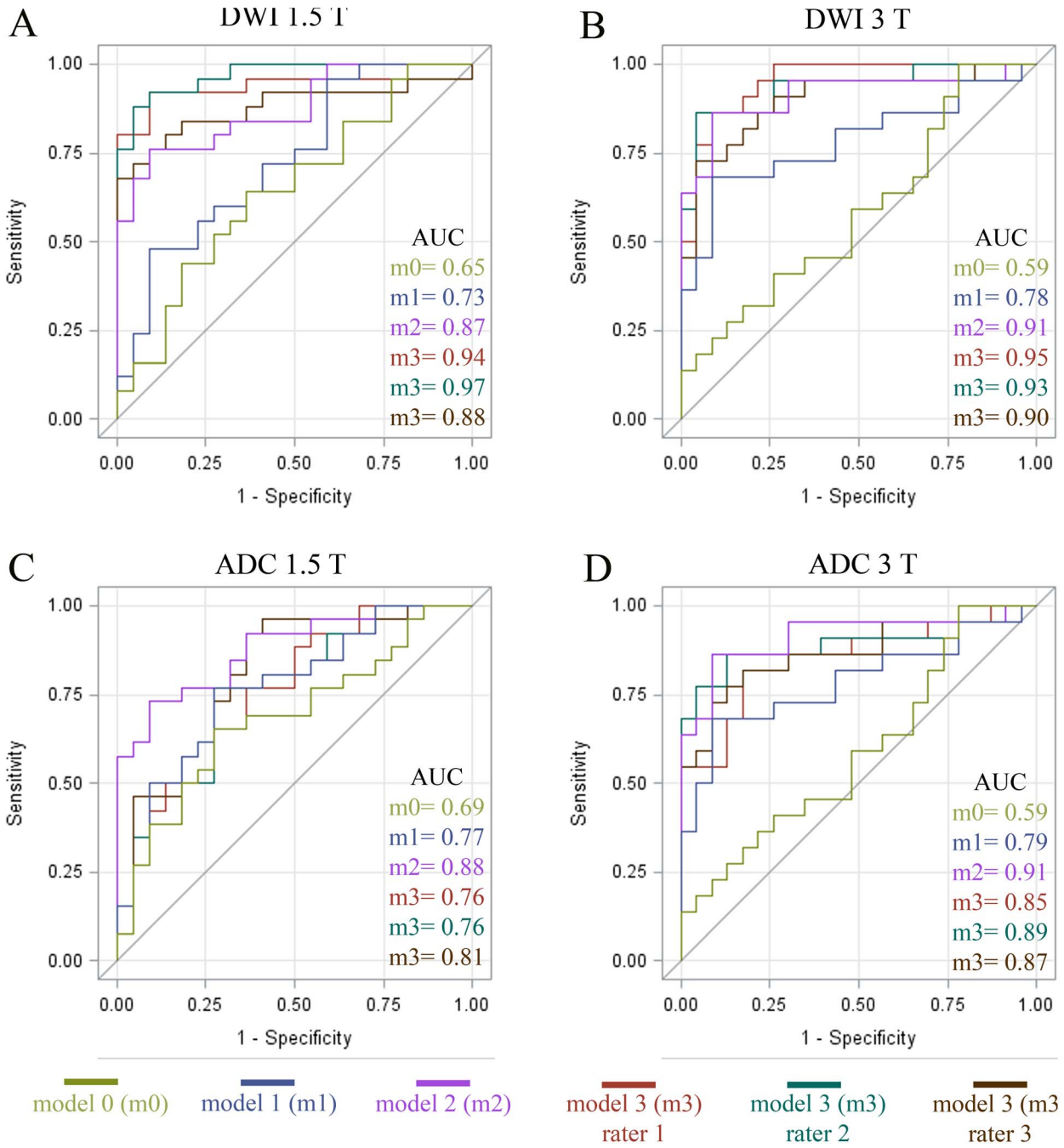

Figure 3. Adjusted ROC curves for the detection of presence of FLAIR-lesions by a relative DWI- and ADC-threshold. ROC-curves belonging to the detailed data presented in table 3 and 4 (please see legends of table 3 and 4 for further details). DWI-models for Group A (1.5 T) and B (3 T) (A,B) and ADC-models for Group A and B (C,D).
doi:10.1371/journal.pone.0092295.g003

assessment of FLAIR imaging is prone to a subjective bias, especially in a clinical setting, where less rigid algorithms are applied to image rating. Despite of these findings, FLAIR imaging is an important clinical tool for the stratification of acute stroke patients and may be supported by other MRI parameters in clinical decision making in the future.

In contrast to DWI, ADC maps were not able to predict the time-dependent appearance of corresponding FLAIR lesions in acute stroke and showed no association with time-from-stroke-onset. Therefore, our results suggest that DWI intensity follows a time-dependent increase in intensity, while ADC-values do not. Several studies have described serial changes of ADC-values and DWI-intensity in acute human stroke, but focused on changes between the (hyper)acute, subacute or chronic stage. ADC values were reported to decrease in the acute stage and to increase again in the subacute and chronic stages [24–29]. DWI values were reported to increase between the acute and subacute stage [27] and to decrease in the chronic stage [30]. There is a substantial lack of knowledge regarding the evolution of DWI and ADC value changes *within* the acute phase of stroke. Based on these

Table 3. Detailed results of the adjusted ROC analysis for DWI and all 3 raters at 1.5 and 3 T.

	AUC(95% CI)	P for comparison with m1	P for comparison with m2
1.5 T (n = 47)			
Model 0 (m0)[a]	0.65 (0.49–0.81)	0.245	
Model 1 (m1)[b]	0.73 (0.59–0.88)		
Model 2 (m2)[c]	0.87 (0.78–0.97)	0.033	
Rater 1 model 3 (m3)[d]	0.94 (0.87–1.00)	0.004	0.075
Rater 2 m3[d]	0.97 (0.93–1.00)	<0.001	0.020
Rater 3 m3[d]	0.88 (0.77–0.98)	0.040	0.760
3 T (n = 45)			
m0[a]	0.59 (0.42–0.76)	0.017	
m1[b]	0.78 (0.64–0.93)		
m2[c]	0.91 (0.78–0.97)	0.031	
Rater 1 m3[d]	0.95 (0.89–1.00)	0.014	0.343
Rater 2 m3[d]	0.93 (0.86–1.00)	0.019	0.369
Rater 3 m3[d]	0.90 (0.80–0.99)	0.052	0.619

[a]m0: adjusted model, adjusted for lesion volume, sex, thrombolysis, NIHSS).
[b]m1: m0 additionally adjusted for age.
[c]m2: m1 additionally adjusted for time (stroke-to-imaging).
[d]m3: m1 and rater specific DWI-ROI values.
At both 1.5 and 3 T, adding the ROI-values for each rater (model 3[m3]) as a variable led to good accuracy for the prediction of FLAIR-hyperintensities for each rater in comparison with the basic models (m0 and m1). The AUC was comparable to m2, which was based on "time-from-stroke-onset". Lack of a significant difference between m2 and m3 emphasizes the close association between time-from-stroke-onset and relative DWI-values. Please see figure 3 for the respective ROC-curves for each model. AUC, Area under the curve; ROI, Region of Interest.
doi:10.1371/journal.pone.0092295.t003

considerations, we see the need to characterize the evolution of DWI and FLAIR intensity values in humans by serial multi-parametric MRI within the (hyper)acute phase of stroke.

DWI is a composite parameter of diffusion imaging and T2-imaging and thus a surrogate of very early restricted diffusion as well as following edema. ADC, on the other hand, is a

Table 4. Detailed results of the adjusted ROC analysis for ADC and all 3 raters at 1.5 and 3 T.

	AUC(95% CI)	P for comparison with m1	P for comparison with m2
1.5 T (n = 48)			
Model 0 (m0)[a]	0.69 (0.53–0.84)	0.257	
Model 1 (m1)[b]	0.77 (0.63–0.90)		
Model 2 (m2)[c]	0.88 (0.79–0.97)	0.033	
Rater 1 model 3 (m3)[d]	0.76 (0.62–0.90)	0.720	0.036
Rater 2 m3[d]	0.76 (0.63–0.90)	0.817	0.039
Rater 3 m3[d]	0.81 (0.69–0.94)	0.340	0.272
3 T (n = 45)			
m0[a]	0.59 (0.42–0.76)	0.017	
m1[b]	0.79 (0.65–0.93)		
m2[c]	0.91 (0.82–1.00)	0.031	
Rater 1 m3[d]	0.85 (0.74–0.97)	0.249	0.374
Rater 2 m3[d]	0.89 (0.78–1.00)	0.111	0.734
Rater 3 m3[d]	0.87 (0.75–0.98)	0.130	0.455

[a]m0: adjusted model, adjusted for lesion volume, sex, thrombolysis, NIHSS).
[b]m1: m0 additionally adjusted for age.
[c]m2: m1 additionally adjusted for time (stroke-to-imaging).
[d]m3: m1 and rater specific ADC-ROI values.
In contrast to DWI (see table 3), adding the ADC-ROI-values for each rater (model 3[m3]) as a variable led to only a bad to moderate accuracy for the prediction of FLAIR-hyperintensities for each rater in comparison with the basic models (m0 and m1). The AUC was even inferior to m2, which was based on "time-from-stroke-onset". Thus, ADC maps cannot reliably predict FLAIR-hyperintensities in contrast to DWI-maps. Please see figure 3 for the respective ROC-curves for each model. AUC, Area under the curve.
doi:10.1371/journal.pone.0092295.t004

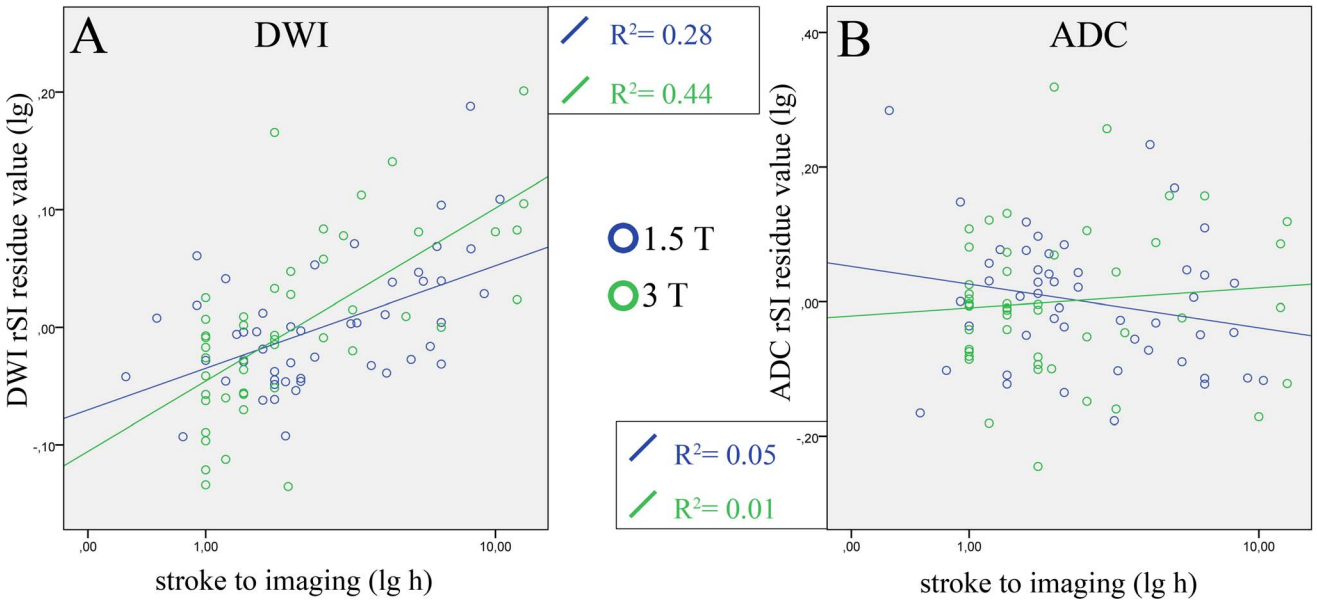

Figure 4. Adjusted linear regression analysis to evaluate the association of relative DWI-intensity and time-from-stroke-onset. Adjusted linear regression analysis was performed to identify a possible association of relative (A) DWI-intensity and (B) ADC-intensity (y-axis,) and time-from-stroke-onset (x-axis) at 1.5 T (blue circles) and 3 T (green circle). At both field strengths, a significant association was found for DWI (A) with moderate adjusted Rsquare values (1.5 T: 0.28; 3 T: 0.44). Adjusted correlation (Spearman's rank correlation) was: 1.5 T = 0.45 ($p<0.001$), 3 T = 0.69 ($p<0.001$). In contrast, no association was found for ADC-maps (B) with adjusted Rsquare values near zero (1.5 T: 0.04; 3 T: 0.01) and weak to no adjusted correlation (1.5 T = −0.22, 3 T = 0.05). Plots are shown in logarithmic scale.
doi:10.1371/journal.pone.0092295.g004

quantification of diffusion alone. In our study, only DWI-intensity thresholds were able to predict the presence of FLAIR-lesions. A possible reason might be the additional information from T2 imaging present in DWI. In this respect, future studies evaluating the time-dependency of DWI from stroke-onset should shed light on the role of diffusion-weighting and T2-weighting as factors of the time-dependent intensity increase.

Importantly, we found that patient age was significantly associated with FLAIR-hyperintensities in both groups. Hence, patient age might be a confounder in the assessment of FLAIR-images for patient stratification in the acute stroke setting. This finding needs investigation to further define the predicition value of qualitative or quantitative FLAIR-imaging.

Our study has several limitations. First, a ROI based approach was chosen instead of a voxel-based analysis. A voxel-based analysis might be more accurate, but ROI-based approaches are less sensitive to spatial distortions occurring in echo planar imaging (EPI). Second, as evidenced by descriptive statistics (s. Table 1), lesion size was heterogenous in both groups, which might include a bias. Third, stroke volumes and stroke severity (based on NIHSS) were only moderate. It remains to be shown, whether our results are also applicable to patient samples with larger mean infarct volumes. Fourth, the patient groups were rather small. Our results should be validated in larger patient samples in future studies. Fifth, comparison of the results obtained at 1.5 T and 3 T is limited by a large time span between the measurements of the study groups. This led to a higher exclusion rate of images due to inferior image quality in the 1.5 T group as a results of advances in MRI techniques. This could have affected the study results. Sixth, owing to mild NIHSS values and small lesion volumes the cohort measured at 3T is not representative for patients eligible for thrombolysis. Our results must therefore be validated for a more diverse patient sample in future studies.

Summary

In conclusion, a relative DWI-intensity threshold predicted the presence of hyperintensities in FLAIR imaging at both 1.5 and 3 T with good accuracy in a retrospective sample. Moreover, DWI-intensity values were associated with time-from-stroke-onset. These findings suggest a time-dependent increase of DWI-intensity in the hyperacute phase of stroke. Future studies should investigate the value of DWI-intensity measurement as an easily accessable estimate of lesion-age.

Acknowledgments

We express our gratitude to the MRI staff of both the Department of Neuroradiology, University of Cologne, and the Academic Neuroradiology, Center for Stroke Research Berlin, Charite Universitätsmedizin Berlin.

Author Contributions

Conceived and designed the experiments: VIM IG WM ME JBF JS. Performed the experiments: VIM IG OZW JBF JS. Analyzed the data: VIM IG UG AS SZM FCvS KLS MAM. Wrote the paper: VIM IG OZW FCvS WM ME JBF JS UG.

References

1. Thomalla G, Cheng B, Ebinger M, Hao Q, Tourdias T, et al. (2011) DWI-FLAIR mismatch for the identification of patients with acute ischaemic stroke within 4·5 h of symptom onset (PRE-FLAIR): a multicentre observational study. Lancet Neurol 10: 978–986. doi:10.1016/S1474-4422(11)70192-2.

2. Aoki J, Kimura K, Iguchi Y, Shibazaki K, Sakai K, et al. (2010) FLAIR can estimate the onset time in acute ischemic stroke patients. J Neurol Sci 293: 39–44. doi:10.1016/j.jns.2010.03.011.
3. Ebinger M, Galinovic I, Rozanski M, Brunecker P, Endres M, et al. (2010) Fluid-Attenuated Inversion Recovery Evolution Within 12 Hours From Stroke Onset: A Reliable Tissue Clock? Stroke 41: 250–255. doi:10.1161/STROKEAHA.109.568410.
4. Petkova M, Rodrigo S, Lamy C, Oppenheim G, Touzé E, et al. (2010) MR imaging helps predict time from symptom onset in patients with acute stroke: implications for patients with unknown onset time. Radiology 257: 782–792. doi:10.1148/radiol.10100461.
5. Galinovic I, Puig J, Neeb L, Guibernau Lisitano J, Kemmling A, et al. (2014) Visual and Region of Interest-based Inter-Rater Agreement in the Assessment of the Diffusion-Weighted Imaging-Fluid-Attenuated Inversion Recovery Mismatch. Stroke, 2014 Feb 20 [epub ahead of print]
6. Ziegler A, Ebinger M, Fiebach JB, Audebert HJ, Leistner S (2011) Judgment of FLAIR signal change in DWI–FLAIR mismatch determination is a challenge to clinicians.J Neurol. Available: http://www.springerlink.com/content/623w4k071r6681g2/. Accessed 7 November 2011.
7. Khademi A, Venetsanopoulos A, Moody AR (2012) Robust White Matter Lesion Segmentation in FLAIR MRI. IEEE Trans Biomed Eng 59: 860–871. doi:10.1109/TBME.2011.2181167.
8. Lansberg MG, Lee J, Christensen S, Straka M, Silva DAD, et al. (2011) RAPID Automated Patient Selection for Reperfusion Therapy A Pooled Analysis of the Echoplanar Imaging Thrombolytic Evaluation Trial (EPITHET) and the Diffusion and Perfusion Imaging Evaluation for Understanding Stroke Evolution (DEFUSE) Study. Stroke 42: 1608–1614. doi:10.1161/STROKEAHA.110.609008.
9. Cizek J, Herholz K, Vollmar S, Schrader R, Klein J, et al. (2004) Fast and robust registration of PET and MR images of human brain. NeuroImage 22: 434–442. doi:10.1016/j.neuroimage.2004.01.016.
10. Randolph JJ (2005) Free-marginal multirater kappa: An alternative to Fleiss' fixed-marginal multirater kappa. Paper presented at the Joensuu University Learning and Instruction Symposium 2005, Joensuu, Finland. Available: http://citeseerx.ist.psu.edu/viewdoc/download?doi = 10.1.1.59.8776&rep = rep1&type = pdf.
11. Brennan RL, Prediger DJ (1981) Coefficient Kappa: Some Uses, Misuses, and Alternatives. Educ Psychol Meas 41: 687–699. doi:10.1177/001316448104100307.
12. Landis JR, Koch GG (1977) The measurement of observer agreement for categorical data. Biometrics 33: 159–174.
13. YOUDEN WJ (1950) Index for rating diagnostic tests. Cancer 3: 32–35.
14. DeLong ER, DeLong DM, Clarke-Pearson DL (1988) Comparing the areas under two or more correlated receiver operating characteristic curves: a nonparametric approach. Biometrics 44: 837–845.
15. Guidelines for Management of Ischaemic Stroke and Transient Ischaemic Attack 2008 (2008). Cerebrovasc Dis 25: 457–507. doi:10.1159/000131083.
16. Adams HP, Zoppo G del, Alberts MJ, Bhatt DL, Brass L, et al. (2007) Guidelines for the Early Management of Adults With Ischemic Stroke A Guideline From the American Heart Association/American Stroke Association Stroke Council, Clinical Cardiology Council, Cardiovascular Radiology and Intervention Council, and the Atherosclerotic Peripheral Vascular Disease and Quality of Care Outcomes in Research Interdisciplinary Working Groups: The American Academy of Neurology affirms the value of this guideline as an educational tool for neurologists. Stroke 38: 1655–1711. doi:10.1161/STROKEAHA.107.181486.
17. Elliott WJ (1998) Circadian Variation in the Timing of Stroke Onset A Meta-analysis. Stroke 29: 992–996. doi:10.1161/01.STR.29.5.992.
18. Sobesky J (2012) Refining the mismatch concept in acute stroke: lessons learned from PET and MRI. J Cereb Blood Flow Metab 32: 1416–1425. doi:10.1038/jcbfm.2012.54.
19. Schaefer PW, Grant PE, Gonzalez RG (2000) Diffusion-weighted MR Imaging of the Brain1. Radiology 217: 331–345.
20. Cheng B, Brinkmann M, Forkert ND, Treszl A, Ebinger M, et al. (2012) Quantitative measurements of relative fluid-attenuated inversion recovery (FLAIR) signal intensities in acute stroke for the prediction of time from symptom onset. J Cereb Blood Flow Metab. Available: http://www.nature.com/jcbfm/journal/vaop/ncurrent/full/jcbfm2012129a.html. Accessed 28 November 2012.
21. Song SS, Latour LL, Ritter CH, Wu O, Tighiouart M, et al. (2012) A Pragmatic Approach Using Magnetic Resonance Imaging to Treat Ischemic Strokes of Unknown Onset Time in a Thrombolytic Trial. Stroke 43: 2331–2335. doi:10.1161/STROKEAHA.111.630947.
22. Heiss W-D, Sobesky J, Smekal U v., Kracht LW, Lehnhardt F-G, et al. (2004) Probability of Cortical Infarction Predicted by Flumazenil Binding and Diffusion-Weighted Imaging Signal Intensity: A Comparative Positron Emission Tomography/Magnetic Resonance Imaging Study in Early Ischemic Stroke. Stroke 35: 1892–1898. doi:10.1161/01.STR.0000134746.93535.9b.
23. Emeriau S, Serre I, Toubas O, Pombourcq F, Oppenheim C, et al. (2013) Can Diffusion-Weighted Imaging–Fluid-Attenuated Inversion Recovery Mismatch (Positive Diffusion-Weighted Imaging/Negative Fluid-Attenuated Inversion Recovery) at 3 Tesla Identify Patients With Stroke at <4.5 Hours? Stroke 44: 1647–1651. doi:10.1161/STROKEAHA.113.001001.
24. Warach S, Gaa J, Siewert B, Wielopolski P, Edelman RR (1995) Acute human stroke studied by whole brain echo planar diffusion-weighted magnetic resonance imaging. Ann Neurol 37: 231–241. doi:10.1002/ana.410370214.
25. Schlaug G, Siewert B, Benfield A, Edelman RR, Warach S (1997) Time course of the apparent diffusion coefficient (ADC) abnormality in human stroke. Neurology 49: 113–119. doi:10.1212/WNL.49.1.113.
26. Schwamm LH, Koroshetz WJ, Sorensen AG, Wang B, Copen WA, et al. (1998) Time Course of Lesion Development in Patients With Acute Stroke Serial Diffusion- and Hemodynamic-Weighted Magnetic Resonance Imaging. Stroke 29: 2268–2276. doi:10.1161/01.STR.29.11.2268.
27. Lansberg MG, Thijs VN, O'Brien MW, Ali JO, Crespigny AJ de, et al. (2001) Evolution of Apparent Diffusion Coefficient, Diffusion-weighted, and T2-weighted Signal Intensity of Acute Stroke. Am J Neuroradiol 22: 637–644.
28. Fiebach JB, Jansen O, Schellinger PD, Heiland S, Hacke W, et al. (2002) Serial analysis of the apparent diffusion coefficient time course in human stroke. Neuroradiology 44: 294–298. doi:10.1007/s00234-001-0720-8.
29. Srivastava A, Mehrotra G, Bhargava S, Agarwal S, Tripathi R (2008) Studies on the time course of apparent diffusion coefficient and signal intensities on T2- and diffusion-weighted MR Imaging in acute cerebral ischemic stroke. J Med Phys 33: 162. doi:10.4103/0971-6203.44479.
30. Eastwood JD, Engelter ST, MacFall JF, Delong DM, Provenzale JM (2003) Quantitative Assessment of the Time Course of Infarct Signal Intensity on Diffusion-Weighted Images. AJNR Am J Neuroradiol 24: 680–687.

Lebenslauf

Mein Lebenslauf wird aus datenschutzrechtlichen Gründen in der elektronischen Version meiner Arbeit nicht veröffentlicht.

Publikationsliste

Ultrahigh-Field MRI in Human Ischemic Stroke – a 7 Tesla Study

Vince I. Madai, Federico C. von Samson-Himmelstjerna, Miriam Bauer, Katharina L. Stengl, Matthias A. Mutke, Elena Tovar-Martinez, Jens Wuerfel, Matthias Endres, Thoralf Niendorf, Jan Sobesky

PLOS One, 2012

7(5):e37631. doi: 10.1371/journal.pone.0037631. Epub 2012 May 31.

Clinical Evaluation of an Arterial-Spin-Labeling Product Sequence in Steno-Occlusive Disease of the Brain

Matthias A. Mutke , Vince I. Madai , Federico C. von Samson-Himmelstjerna, Olivier Zaro Weber, Gajanan S. Revankar, Steve Z. Martin, Katharina L. Stengl, Miriam Bauer, Stefan Hetzer, Matthias Günther, Jan Sobesky.

PLOS One, 2014

Feb 6;9(2):e87143. doi: 10.1371/journal.pone.0087143. eCollection 2014.

DWI Intensity Values Predict FLAIR Lesions in Acute Ischemic Stroke

Vince I. Madai, Ivana Galinovic, Ulrike Grittner, Olivier Zaro-Weber, Alice Schneider, Steve Z. Martin, Federico C. v. Samson-Himmelstjerna, Katharina L. Stengl, Matthias A. Mutke, Walter Moeller-Hartmann, Martin Ebinger, Jochen B. Fiebach, Jan Sobesky.

PLOS One, 2014

Mar 21;9(3):e92295. doi: 10.1371/journal.pone.0092295. eCollection 2014.

3D GRASE pulsed arterial spin labeling at multiple inflow times in patients with long arterial transit times: comparison with dynamic susceptibility-weighted contrast-enhanced MRI at 3 Tesla

Steve Z. Martin, Vince I. Madai, Federico C. von Samson-Himmelstjerna, Matthias A. Mutke, Miriam Bauer, Cornelius X. Herzig, Stefan Hetzer, Matthias Günther and Jan Sobesky.

Journal of Cerebral Blood Flow & Metabolism, 2015

Mar;35(3):392-401. doi: 10.1038/jcbfm.2014.200. Epub 2014 Nov 19.

Correction for Susceptibility Distortions Increases the Performance of Arterial Spin Labeling in Patients with Cerebrovascular Disease

Vince I. Madai, Steve Z. Martin, Federico C. v. Samson-Himmelstjerna, Cornelius X. Herzig, Matthias A. Mutke, Carla N. Wood, Thoralf Thamm, Sarah Zweynert, Miriam Bauer, Stefan Hetzer, Matthias Günther, Jan Sobesky.

Journal of Neuroimaging, 2016

Jan 27. doi: 10.1111/jon.12331. [Epub ahead of print].

Danksagung

Ich danke vor allem meinem Doktorvater Prof. Dr. med. Jan Sobesky, der mich mit seinem Enthusiasmus für die Schlaganfallbildgebung immer begleitet hat und Dr. med. Vince Madai für seine Betreuung und stetigen Beistand.

Ich danke zudem besonders Dipl. Phys. Federico von Samson-Himmelstjerna, PD Dr. med. Olivier Zaro Weber, meinen Mitdoktoranden Steve Martin und Cornelius Herzig und nicht zuletzt Miriam Bauer, Andrea Hassenpflug und allen Coautoren.

Ich bedanke mich bei meinen lieben Eltern und meinem Bruder für ihre ständige Unterstützung.